CHALMERS
UNIVERSITY OF TECHNOLOGY

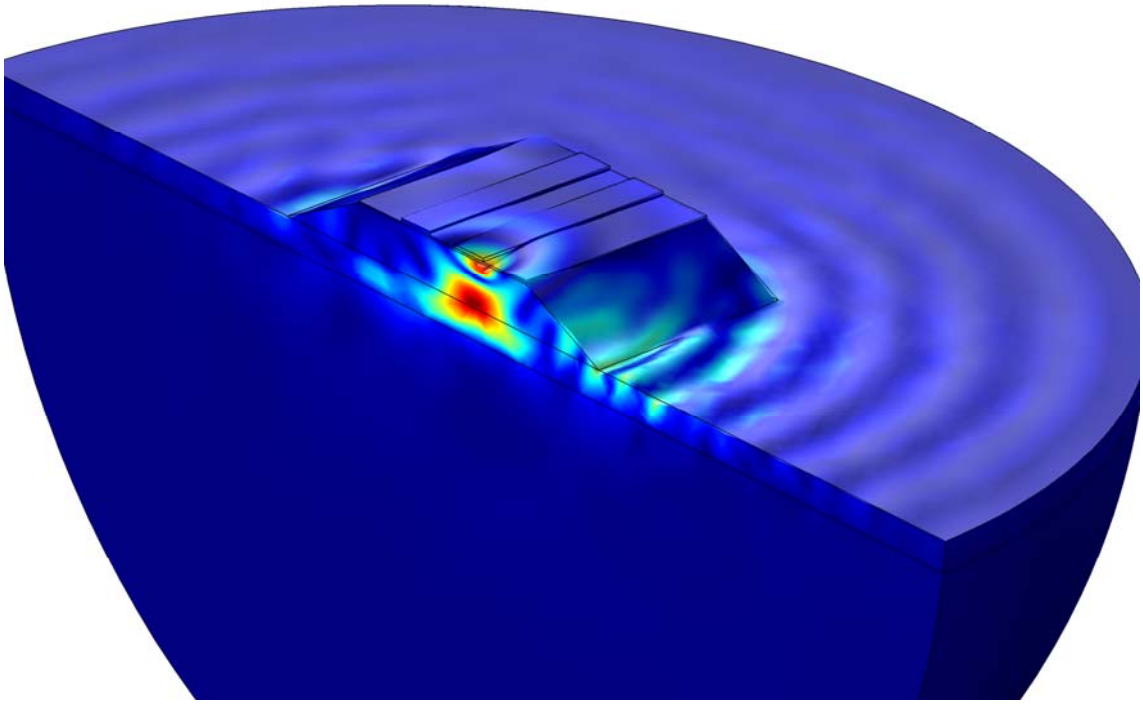

Effect of Slow Process in Soft Soil on the Dynamic Response of High-Speed Railway Foundation

Master's Thesis in Structural Engineering and Building Technology / Sound and Vibration

IBRAHIM RASHID
MEIHUI TAO

Department of Civil and Environmental Engineering
Division of Geo Engineering / Division of Applied Acoustics
Geotechnical Engineering / Vibroacoustics Group
CHALMERS UNIVERSITY OF TECHNOLOGY
Master's Thesis BOMX02-16-90
Gothenburg, Sweden 2016

Master's thesis in Structural Engineering and Building Technology / Sound and Vibration

Effect of Slow Process in Soft Soil on the Dynamic Response of High-speed Railway Foundation

IBRAHIM RASHID
MEIHUI TAO

CHALMERS

Department of Civil and Environmental Engineering
Division of Geo Engineering / Division of Applied Acoustic
Chalmers University of Technology
Gothenburg, Sweden 2016

Effect of Slow Process in Soft Soil on the Dynamic Response of High-speed Railway Foundation
IBRAHIM RASHID
MEIHUI TAO

Master's Thesis BOMX02-16-90
Department of Civil and Environmental Engineering
Division of Geo Engineering / Division of Applied Acoustics
Chalmers University of Technology
SE-412 96 Gothenburg
Telephone +46 31 772 1000

Cover: Vertical displacement field of the combined model at 10 Hz

Gothenburg, Sweden 2016

Effect of Slow Process in Soft Soil on the Dynamic Response of High-speed Railway Foundation
Master's thesis in Structural Engineering and Building Technology / Sound and Vibration
IBRAHIM RASHID
MEIHUI TAO
Department of Civil and Environmental Engineering
Division of Geo Engineering / Division of Applied Acoustic
Chalmers University of Technology

Abstract

High-speed trains with speeds of 300-320 km/h are planned to be developed in Sweden. In the west coast of Sweden, the soil is mainly comprised of soft clay. This could lead to both vibration and long-term settlement problems. The aim of this thesis is to analyse the creep behavior of soft clay and the dynamic response during the service life of the railway foundation, which will be an embankment, and the surrounding ground.

Two separate models of railway foundation were simulated and studied by using PLAXIS 2D for the settlement and COMSOL Multiphysics for the dynamic component. In order to consider the degradation of soil properties, the strain distribution calculated from the static model in PLAXIS 2D was exported into the dynamic model. Thereafter, the changed shear modulus and loss factor were obtained.

The settlement predicted by the PLAXIS 2D model due to solely the embankment weight is approximately 500 mm which is considerably greater than the allowed one by Trafikverket which is 30 mm. It was expected as no ground improvements were considered, especially in this case as the soil is soft clay.

The dynamic study shows that, due to the small changes in shear modulus distribution during the service life of the embankment, there are no major differences on the dynamic response of the embankment. A decrease in vibration levels on the ground surface further from the embankment occurs as time goes by. However, the model has limitations in its geometry and mesh precision which prevents from more detailed conclusions being drawn.

The thesis shows a possible way of combining geotechnical and ground vibration studies by considering the changed moduli and loss factor of soil during the slow process in the dynamic analysis.

Keywords: Ground - structure dynamics, Soft soil, Creep-SCLAY1, High-speed railway foundation

Acknowledgements

This MSc-thesis was initiated by the authors and was supported by the Division of GeoEngineering, Divison of Applied Acoustics at Chalmers University of Technology, and WSP | Parsons Brinckerhoff in Gothenburg. The examiners and supervisors were Dr. Jelke Dijkstra and Dr. Patrik Höstmad from Chalmers University of Technology, and Per Friberg and Johan Scheuner from WSP | Parsons Brinckerhoff.

We would like to express our deepest appreciation to our supervisors for the guidance and help throughout this thesis. Without their support, this thesis would not have been possible. We would also like to thank Professor Minna Karstunen and Dr. Mats Olsson for their valuable advices.

We would also like to dedicate our special thanks to the Ph.D students at the Division of GeoEngineering at Chalmers University of Technology for their positive energy and friendship which have helped us directly and indirectly through this project.

We would like to thank Matilda Arnesson and Andreas Holmqvist for the detailed feedback on the thesis, and Professor L. Grau from INSA Lyon for providing more information on his publications.

Ibrahim would like to express his deepest appreciation to Naomi Licudi for her precious support and encouragement. Meihui would like to express her thanks to class 2014 - 2016 from Division of Applied Acoustics, for the long-lasting friendship and company of the past two years.

Last but not least, we would like to thank our family and friends for their endless love and support.

Ibrahim Rashid, Meihui Tao, Gothenburg, June 2016

Contents

List of Notifications

Abbreviations

CSR	Cyclic stress ratio
MASW	Multichannel analysis of surface waves
OCR	Overconsolidation ratio

Greek letters

α_0	Initial value of anisotropy
α_{Ko}^{NC}	Rotational hardening parameter for normally consolidated soil
β	Creep ratio
χ	Volumetric strain
χ_0	Initial amount of bonding
χ_d	Deviatoric strain
$\dot{\epsilon}_v$	Creep strain rate
$\dot{\Lambda}$	Visco-plastic multiplier
η	Isotropic loss factor
η_{Ko}^{NC}	Stress ratio in normally consolidated state
γ_a	Strain amplitude

γ_c	Cyclic shear strain
γ_s, γ	Shear strain
κ^*	Modifield swelling index
λ	The first lame parameter
λ^*	Modifield compression index
μ	The second lame parameter
μ^*	Modifield creep index
ν	Poissin ratio
ω	Rate of rotation
ω_d	Rate of rotation due to deviatoric strain
ρ	Density
τ	Reference time

Roman letters

D	Damping ratio
d	Mechanical impedance in COMSOL
E	Young's modulus
e	Void ratio
f	Frequency
G	Shear modulus
G_0	Small strain shear modulus

h	Thickness of certain components
I_p	Plasticity index
K	Bulk modulus
M	Slope of critical state line
M_c	Stress ratio at critical state trixial in compression
M_e	Stress ratio at critical state trixial in extensionn
N	Number of cycles
$P-wave$	Compression wave
$S-wave$	Shear wave
S_r	Degree of saturation
u	Pore water pressure
V_c, c_p	P-wave velocity
V_s, c_s	Shear wave velocity
W_L	Liquid limit
W_n	Natural water content
W_p	Plasticity limit

List of Figures

List of Tables

Chapter 1

Introduction

1.1 Background

Politicians have decided to improve the accessibility among the main cities in Sweden. This will be achieved by expanding the infrastructure and building new connections such as roads, railways, tunnels and bridges. Several high-speed railway lines with a maximum speed of 320 km/h will be developed, as shown in Figure 1.1. In the future, it will be possible to travel between Stockholm and Göteborg in 2.0 hours and between Stockholm-Malmö in 2.5 hours (Trafikverket, 2015).

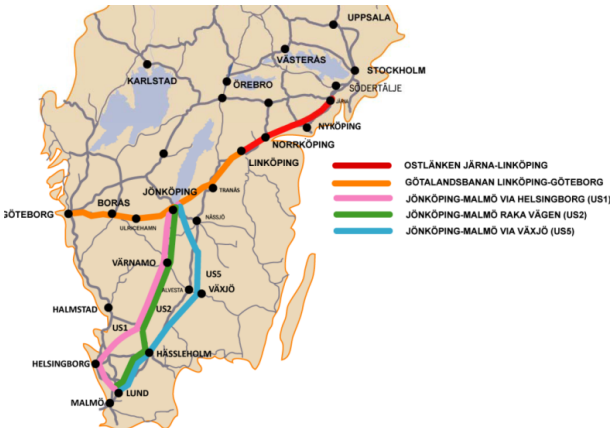

Figure 1.1: Plans of future high-speed railways in Sweden (Uneklint & Bernström, 2015)

Trafikverket which is the Swedish Transport Administration has set a number of requirements for the high-speed train (Axelsson, 2016):

- Maximum speed of 320 km/h
- Up to 10 trains per hour
- Axle load of the train, approximately 17 tons
- Total settlements after 120 years, < 30 mm

- Service life, 120 years
- Ballast free foundation

This project will focus on regions where the soil is composed of a high amount of soft clay. This type of soil can cause problems for a high-speed train constructions. When the train speed exceeds the critical wave speed of the track, the soft soil is subject to a drastically increased dynamic load. In the long term, this load could lead to accelerated deformation. It is important to understand the dynamic load per train cycle, how the clay behaves under the cycling loads and the soil property changes in the long term.

Since Trafikverket has not decided yet which type of track foundation will be used, concrete slab is assumed in the calculations, which is recommended by Trafikverket (Axelsson, 2016).

1.2 Objective

The aim of this research is to analyse the creep behavior of soft soil, and its effect in the dynamic response of a railway foundation for high-speed trains. The study is based on computer simulation, and assumptions have been made on the soil properties, the structure of railway foundation, etc. The goal of this research is to make an attempt to combine geotechnical studies with vibration studies, and gain some general understanding on both subjects.

The target results of the simulation is (1) the settlement of the foundation after 120 years without any soil reinforcement, and (2) the dynamic response of the foundation. The simulation results are chosen to demonstrate that the method of combining two subjects could provide reasonable values, and therefore would be preliminary, since a number of assumptions and simplifications are made in the calculation, and no experimental work has been done to validate the results.

In this thesis, the dynamic response of railway foundation was studied under an impact load excitation; the effect of a moving load was not studied due to time limitation. Also to simplify the problem, the dynamic response is calculated with a linear elastic model.

1.3 Thesis structure

The thesis consists of 3 major parts: theories, constitutive models from the geotechnical and vibrational perspective, and a model combining the two perspectives. The work flow is shown in Figure 1.2.

In Chapter 2, the theoretical background obtained through literature studies for both the settlement and vibration studies are presented.

After the fundamental understanding of the respective domains, two different constitutive model were simulated. For the settlement, PLAXIS 2D was utilized. A creep model developed by Nallathamby Sivasithamparam, Minna Karstunen, Paul Bonnier was used

to study the behavior of clay after 120 years, which is the service life of the railway foundation for high-speed trains. This model is presented in Chapter 3.

For the vibration, COMSOL Multiphysics software has been utilized. A simplified model of one concrete slab resting on a two-layered half-space was created. The result of this model was verified with an analytical solution published by Grau (2015). This model is presented in Chapter 4.

The PLAXIS 2D and the COMSOL Multiphysics constitutive models were combined to study the dynamic response of the railway foundation. The implementation of the combined model as well as the results are presented in Chapter 5.

The results are summarised and discussed in Chapter 6, and recommendations for future work is presented in Chapter 7.

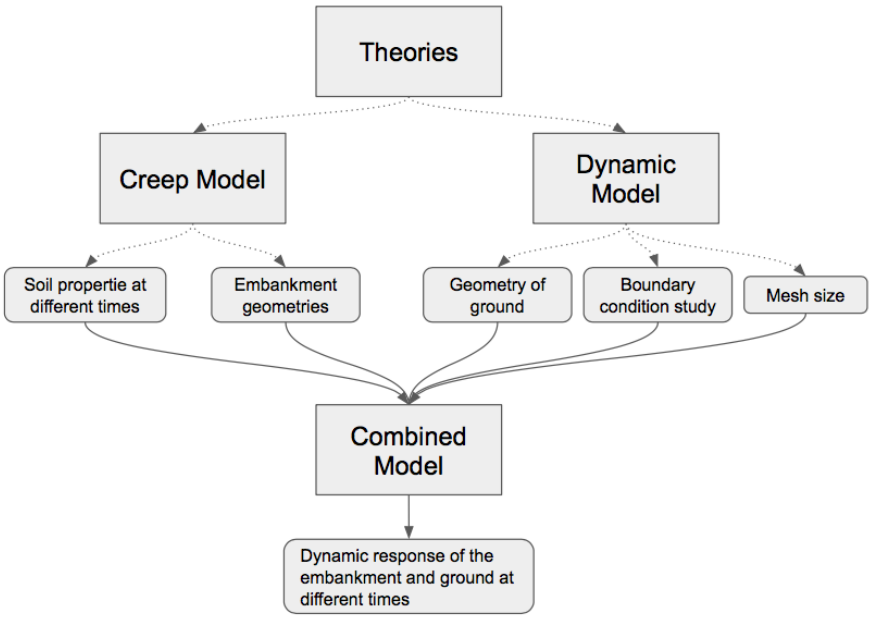

Figure 1.2: The work flow for this master thesis

Chapter 2

Theories and literature study

In this chapter, the relevant theories and background knowledge related to track structures, the behavior of soft soil, railway-induced vibrations, and finite element modelling are presented.

2.1 Design of common track structures

In general, the design of a railway structure includes tracks, fasteners, sleepers, ballast (or slab), and the underlying subgrade. Depending on which type of structure the tracks rest on, they are divided into two catagories (Track structure n.d.):

1. traditional track structure (ballasted track)
2. ballastless track

Traditional ballasted railway

The traditional ballasted railway has been the dominating design for railways since the beginning of 1900s. In this type of rail, the track is connected to sleepers, which rest on a pile of crushed stones - the ballast. The purpose of the ballast is to support the sleepers while allowing subtle adjustment of their position, and to have free drainage.

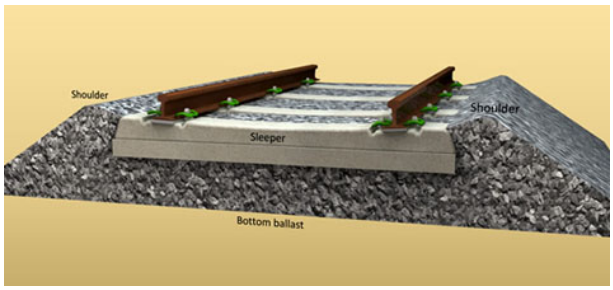

Figure 2.1: Traditional ballasted rail (Track structure n.d.)

The track is connected to sleepers using spikes, with elastic pad in between. There are also springs called 'tension washers' to provide some isolation between the track and sleepers.

Ballastless rail

In ballastless rail, tracks are mounted directly on a slab, which is usually made of concrete. This type of rail is known for its long life cycle, and its ability to support high speed trains.

In this thesis, a ballastless rail with a concrete slab is studied, which is assumed to be the future high-speed railway in Sweden.

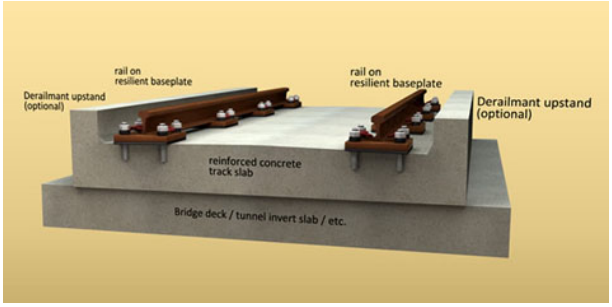

Figure 2.2: Ballastless rail (Track structure n.d.)

2.2 Behavior of soft soil

The behavior of soft soil is highly affected by the historical events such as sedimentation, geological deposition and human activity. The maximum effective stress which a soil has been subjected to is defined as the preconsolidation stress (Länsivaara, 1999). This parameter is a governing factor for determining the deformation of clay. During laboratory test, it has been determined that the preconsolidation pressure is affected by the strain rate, as it increases, the preconsolidation pressure also increases. The overconsolidation ratio (OCR) is the ratio between the current effective stress and the preconsolidation stress. If it has the same magnitude as the preconsolidation stress then the clay is considered to be normally consolidated. This occurs after equilibrium is reached by its own weight (Bjerrum, 1973). If the magnitude of the current effective stress is lower than the preconsolidation stress it is said the clay is overconsolidated.

Consolidation is a time related process of soil deformation, this process is divided into two different categories: primary and secondary consolidation.

According to Terzaghi (Kellett, 1974), primary consolidation is the process where saturated soil decreases in volume under loading due to water expulsion without replacement by air. Under cyclic loading, consolidation deformation is larger than for static loading which could partially be due to creep that occur when the cyclic loading is applied (Tang, 2013). The magnitude of creep is proportional to cyclic load magnitude, loading period, load increment ratio and the amount of organic content in the soil (Mohammad M. Toufigh, 2009). For soils with low permeability such as clay, the water dissipates slower so the deformation is time dependent. An increase in external stress on a soil which contains clay will create an excess of pore water pressure (Länsivaara, 1999).

The secondary consolidation which is also referred to as creep deformation or plastic resistance to compression (Larsson, 1986) occurs when the pore water pressure has dissipated and the applied load is exposed to the clay structure. This creep deformation is due to

viscous deformations which begin during primary consolidation and the re-packing over time of particles to aggregates (Hansbo, 1975). The strength which is created between the aggregate will increase the deformation resistance. This will slow down deformation and it will eventually reach zero. This type of consolidation is a slow deformation when compared to the primary consolidation.

2.2.1 Deformation of soft clay under cyclic loading

Soft soil which is subjected to cyclic loading can be either elastically or plastically deformed. The former is recoverable whilst the latter is not and has an accumulation effect. When a soil is subjected cyclically to loading and unloading, the soil will only recover a small part of the compression during the unloading process. Therefore, the soil will be permanently deformed (Tang, 2013).

The deformation magnitude depends on the number of loading amplitude and periods. An accumulated residual, plastic, deformation affects the service life of the foundation. For determining the settlement of a soil which is subjected to cyclic loading, two methods are used. The first one is based on practical experience whilst the second method is based on the elastoplastic constitutive model.

The residual deformation is influenced by a number of parameters such as cyclic stress ratio (CSR), loading frequency, consolidation state and confining pressure.

2.2.2 Behavior of clay in Gothenburg region

The behavior of the clay in the Gothenburg region varies greatly and therefore it is not correct to refer to "Behavior of the Gothenburg clay". It depends on numerous factors such as human activities and to natural events such as geological deposition, geological unloading due post glacial erosion and different landslides that have occurred. Due to geological deposition, the soil is highly dominated by layers of post-glacial marine clay which can be caused by changes of the sea level (Länsivaara, 1999). In the region of Gothenburg, a high amount of sensitive clay can be found, which can lose a large amount of its mechanically strength during remolding and disturbance.

In a study where eight sites in Gothenburg were investigated by Wood and Dijkstra (2015). It was demonstrated that the clay varied from normal to over consolidated.

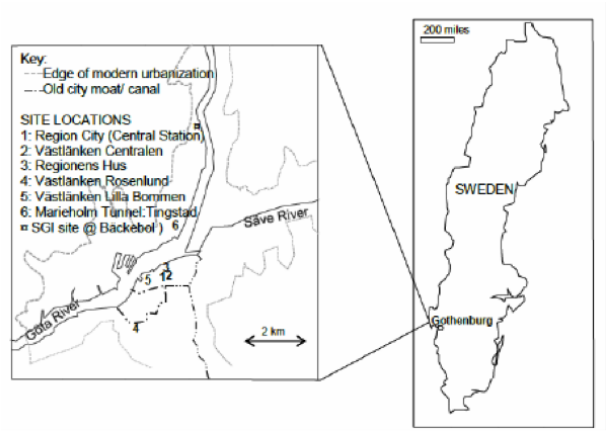

Figure 2.3: Location of the different sites (Wood & Dijkstra, 2015)

For site number one to three, the soil is lightly consolidated where the soil can be described as gyttjig silty clay to sulphide strained silty marine clay with a post glacial geological deposition. Where the soil has a glacial geological deposition it could be seen that the soil contains marine sulphide rich/strained silty clay to marine sulphide varved silty clay. For site number four to six, the soil can be described the same as for the first three sites but it contains more silt. For site number seven, the soil is lightly to normally consolidated. The soil can described as silty clayey gyttja to silty marine clay where the geological deposition was a post glacial origin. For site number eight, the soil is over consolidated and is described as silty sulphide varved distal marine clay. The location of those sites are presented in Figure 2.3. The soil parameters for the different sites are presented in appendix A (Wood & Dijkstra, 2015).

2.2.3 Dynamic properties

According to different prior research estimation of small strain stiffness are not only dependent on the inherent structure of the soil but also on the geological history. Dynamic material parameters are required to predict the stability of soil layers and how it varies with time and cyclic loading. During cyclic loading, the density, plasticity index, overconsolidation ratio, confining effective stress, void ratio and saturation degree are essential for characterization of the soil, predictions of ground movement and field data interpretation (Benz, 2007). The dynamic response of the soil is mainly governed by the following mechanical parameters:

Damping ratio (D)

Damping ratio is defined as the damping coefficient divided by the critical damping. This parameter represents how a soil dissipates dynamic load/energy and how it influences the vibration propagation. Damping ratio is not only influenced by the damping material parameters but also by the shear strain, soil-structure interaction and if it is a single or multi degree modal systems. With increasing the confining stress, the damping in soil is decreasing. If the value of damping ratio is lower than one, the system is underdamped, if it is equal to one it is critically damped and if it is higher than one it is overdamped (Luna

& Jadi, 2000).

Shear modulus (G)

The shear modulus parameter is used for defining the stiffness of a soil and how the interaction of a soil-structure behaves during cyclic loading (dynamic response). This parameter is useful since it is strain dependent and it represents the modulus in a stiffness degradation curve for a saturated soil behavior varying with the strain (Darendeli, 2001). The small strain shear modulus is used to define the relation between the shear modulus and the shear strain. It is influenced by the porosity of the soil, its historical geological past and the confining effective stress (Benz, 2007).

Shear wave velocity (V_s)

Shear waves velocity is mainly influenced by the structure of the soil and the shear stiffness. The breakage and rearrangement of the soil skeleton could lead to a decrease in the shear wave velocity. With increasing depth and number of cyclic loadings, the shear wave velocity decreases (Luna & Jadi, 2000). It can be determined by different methods such as the Bender element test. Once the shear wave velocity is known, the small strain shear modulus can be determined (Asslan, 2008).

Poisson ratio (ν)

The Poisson ratio is an essential property in 2D that describes the relationship between the axial stress and radial strain of a soil. This parameter is difficult to be measured and is in general assumed to have a value between 0.2-0.5. In laboratory, the Poisson ratio can be measured by using an existing dynamic triaxial test. The Poisson ratio is influence by the staturation degree (Luna & Jadi, 2000). If the Poisson ratio and the Young's modulus are known, the bulk modulus (K) and the shear modulus (G) can be determined by the following analytical formulas for small strain:

$$K = \frac{E}{3(1-2\nu)} \tag{2.1}$$

$$G = \frac{E}{2(1+\nu)} \tag{2.2}$$

Lamé's parameters (λ, μ)

Lamé parameters are one set of parameters that fully describes the moduli of an elastic solid. μ is also known as the shear modulus, which is the same as G. They are related to Young's modulus (E) as described by the following equations:

$$\lambda = \frac{\nu E}{(1+\nu)(1-2\nu)}, \quad \mu = \frac{E}{2(1+\nu)} \tag{2.3}$$

2.2.4 Dynamic loading

One of the governing factors in dynamic soil is the frequency of cyclic loading. The strain amplitude varies with range of loading frequencies. During the initial loading cycle, the soil is induced to a quick deformation and it gradually becames slower. That is due to compaction effect of the soil after multiple cycles, the dynamic strain is increasing with time into the strain value reach a stabilization level. During laboratory tests made in China, the deformation induced was larger during low frequency loading compared to high frequencies (Tang, 2013). That can seen from the e-N curve in Figure 2.4. This phenomenon can be due to elasticity properties of the soil. During high loading frequency, the pore water pressure does not have time to dissipate before the next cycle starts, if the loading time is longer than a certain value that could lead to fully pore water pressure dissipation. Critical cyclic stress ratio depends on the cyclic loading, confining pressure and the soil properties. The frequency level has a significant effect on CSR(Cyclic stress ratio), with lowering the loading frequency, CSR increase. At CSR values lower than 0.3, the deformation is in attenuation mode and the soil has a recoverable deformation. For larger CSR value, the soil start to behave more plastic and the residual deformation starts to be accumulated (Tang, 2013). At low loading frequency, the soil structure has enough time to recover but when the frequency increase to a certain level the soil is not able to recover due to short time between the cycles. (Zhang & Toa, 1994), conclude that a lower loading frequency results in a higher pore water pressure accumulation, a higher lateral strain and an increase in damping ratio.

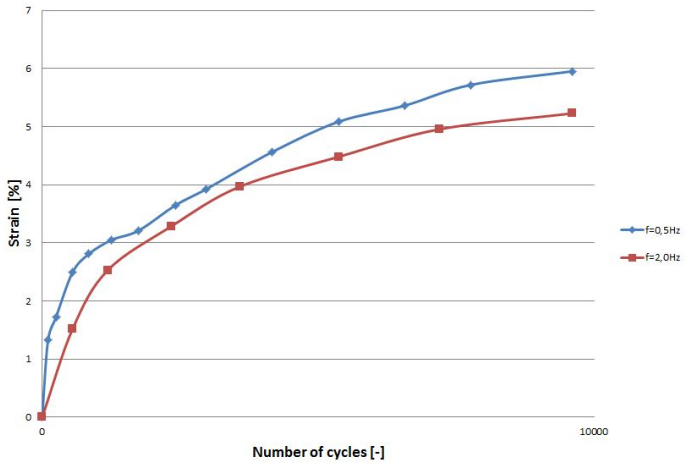

Figure 2.4: ϵ - N curve, CSR=0.4 (Tang, 2013)

The properties of compression waves are mainly governed by water. For saturated soil, P-waves are primarily influenced by the fluid bulk modulus. The bulk modulus and porosity (n), have less influence on the compression wave (Benz, 2007). For soil which contains clay, if the phreatic level is near the surface, the soil can be assumed to be 80 - 90 % saturated. In pure water, the compression wave velocity is measured to 1480 m/s.

Shear waves are highly influenced by the properties of the saturated soil, such as the skeleton stiffness and the density.The saturation degree is the relation of volume of water to the volume of voids. By increasing the degree of saturation, the skeleton stiffness

decreases and that lead to a reduction in shear wave velocity. From measurements of different unsaturated soils with different degrees of saturation and external confining pressures, (Tang, 2013) it was observed that the shear stiffness depends on the saturation degree at a certain peak. It was later on observed that this peak was influenced by the confining pressure.

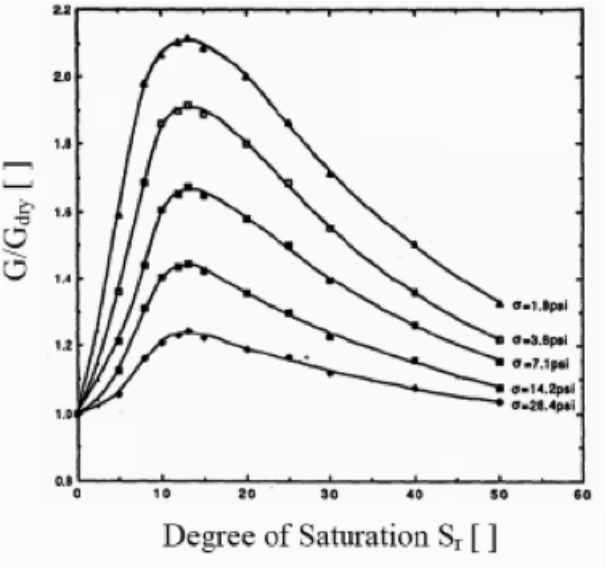

Figure 2.5: Shear stiffness of unsaturated soil depending of confining pressure and degree of saturation (Tang, 2013)

The governing soil parameters in wave propagation are the shear stiffness (G), bulk modulus (K), density (ρ) and the attenuation. Small strain stiffness can be calculated from the following elastodynamics method based on the shear wave velocity and the density of soil.

$$G_0 = \rho V_s^2 \tag{2.4}$$

2.2.5 Stiffness degradation curve

The shear stiffness of a soil is represented by the shear modulus (G). It can be described as the relation between the shear stress (τ) and shear strain (γ). Due to nonlinear behavior between stress and strain, a degradation curve is used. The rigidity of soil at very small strain is characterized by the small strain shear modulus (G_0) (Darendeli, 2001). The modulus ratio is the shear modulus, G, divided by the small strain shear modulus, G_0. The stress-strain properties of the degradation curve are mainly dependent on two parameters: the small strain shear modulus and the shear strain (Benz, 2007).

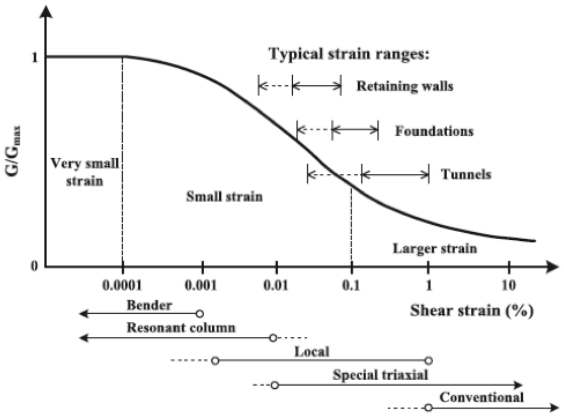

Figure 2.6: Idealized stiffness degradation curve (Likitlersuang, Teachavorasinskuna, Surarakb, Ohc, & Balasubramaniamc, 2013)

During cyclic loading, when the strain amplitude goes above a certain value, the soil will have a permanent loss of strength due to an accumulation of excess pore water pressure (Okura & Ansal, 2007). The reference threshold shear strain is defined as the shear strain at 70 % of the stiffness degradation (G/G_0), where G is the average shear stiffness or secant shear modulus. It represents the degree of non-linearity at medium strain level (Benz, 2007).

It also represents the boundaries of soils during cyclic loading at very small to large shear strain level. These different strain levels are represented in the degradation curve with three different categories depending on strain level, see Figure 2.6 above. The first category (10^{-4} % Shear strain) is present in the elastic region, where there is very small strain and the stiffness modulus remains constant. The response is linear and elastic theory is associated to the material behavior. The damping ratio is small and degradation of secant shear modulus is negligible. For the second category (10^{-2} % Shear strain), the stiffness modulus changes non-linearly with the strain. For the third category (10^{-1} % Shear strain)), there is a large strain level where the soil has a non-linear behavior, the deformation is permanent and eventually the material is on the limit of collapse and the stiffness modulus of the soil is relatively small. The damping ratio is large and the degradation of secant shear modulus is significant (Likitlersuang, Teachavorasinskuna, Surarakb, Ohc, & Balasubramaniamc, 2013).

Several different parameters such as void ratio, mean confining pressure, strain amplitude, degree of saturation, diagenesis, over consolidation ratio, plasticity index and number of cycles influence the small strain stiffness in cohesive soil (Benz, 2007). According to a number of researchers (Hardin & Drnevich, 1972), (Vucetic & Dobry, 1991), (Rampello, Viggiani & Amorosi, 1997), (Darendeli, 2001), the void ratio and the mean effective confining pressure have the greatest influence on small strain stiffness.

The effects of the other parameters mentioned on the small strain stiffness are the following:

- Strain amplitude or loading ratio is directly proportional to the small strain stiffness and is dependent on the plasticity index (Benz, 2007).

- Over consolidation ratio, which is dependent of the number of particle bonds and the current effective stress, has a small influence on the small strain stiffness (Hardin & Drnevich, 1972), (Rampello, Viggiani & Amorosi, 1997), (Darendeli, 2001). The magnitude of how much it affects the G_0 depends on the plasticity index.
- Diagenesis is the process of cementation and aging. These processes change the mechanical properties of soils. Cementation is mainly due to artificial or natural soil stabilization and soils which contain sand are particularly susceptible to this effect. The process of aging describes how the mechanical soil properties are changing with time under constant load amplitude.
- Plasticity index influence on small strain shear modulus is not agreed upon entirely by researchers. A number of researchers assume that the stiffness degradation (G/G_0) increases and the damping ratio decreases when the plasticity of the soil increases, (Hardin & Drnevich, 1972), (Kim & Novak, 1981), (Vucetic & Dobry, 1991), whereas other assumes that G/G_0 decreases with increased plasticity index.

When a soil is subjected to a cyclic load, a hysteresis loop is developed during the loading and unloading process. The shape of the loops depends on the strain magnitude, with an increase of the strain level, the secant shear modulus decrease (Brinkgreve, Kappert, & Bonnier, 2007). This hysteresis loop can be described by two parameters: the shear modulus which is represented by the inclination, and the damping, which is represented by the breadth of the loop. For regular periodic loading, the shear modulus during unloading has the same magnitude as for the initial tangent curve in loading (Figure 2.7, a). The shape of unloading and reloading has the same shape as for the unloading and initial loading but the magnitude is twice as big (Figure 2.7, b). For irregular periodic loading, if the new periodic unloading and reloading curve have higher strain levels than the last cycle, it will follow the unloading curve until the next cycle starts (Figure 2.7, c). If a new periodic loading passes through the previous curve, it follow the previous stress-strain curve, (Figure 2.7, d) (Ebrahimian, 2013).

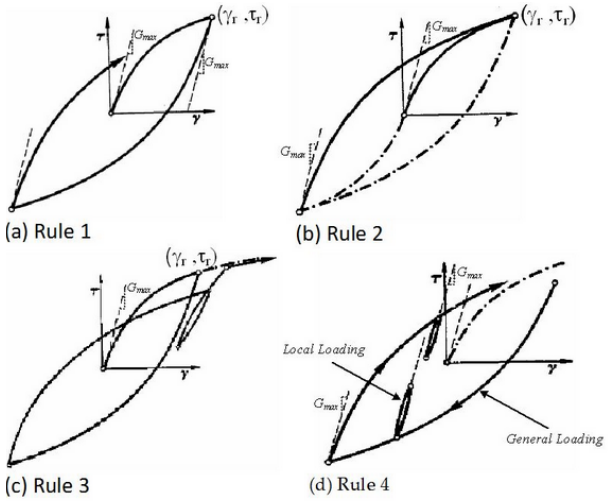

Figure 2.7: Hysteresis loop, Unloading and reloading (Ebrahimian, 2013)

The soil ability to damping of the soil is the opposite of the secant shear modulus. The

damping force increases when the soil stiffness decreases with strain amplitude, see Figure 2.7. That can be explained that due to heat, friction and yielding, the soil dissipates the energy from cyclic loading. It can be seen in Figure 2.8 that the plasticity index has a large influence on the damping ratio and the effect of the void ratio is negligible.

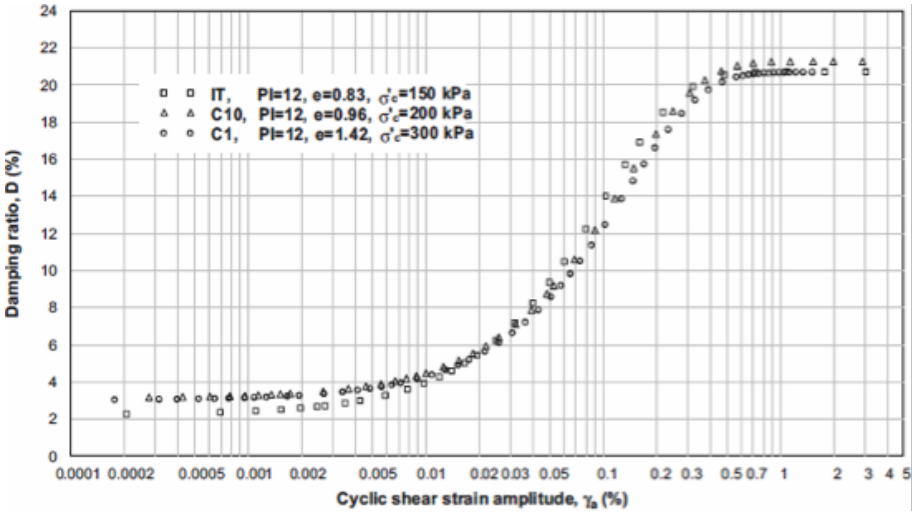

Figure 2.8: Effect of plasticity index on damping ratio (Okura & Ansal, 2007)

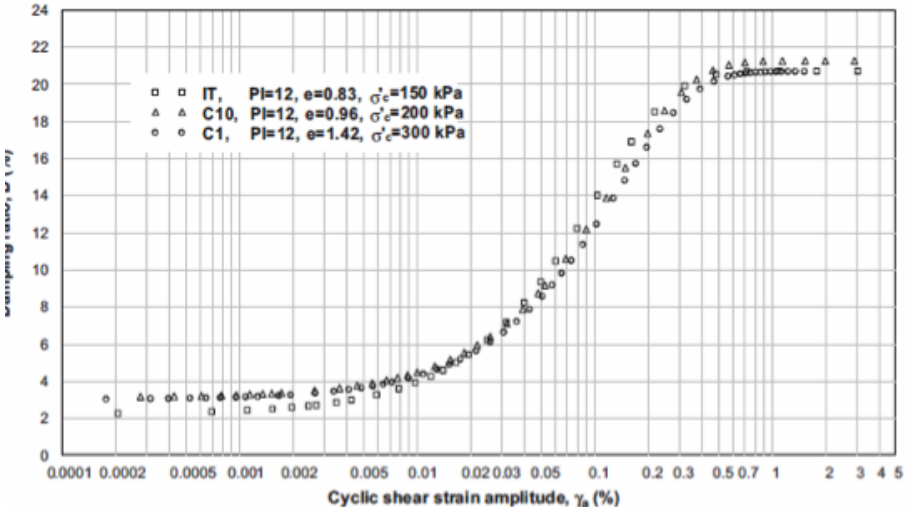

Figure 2.9: Effect of void ratio on damping ratio (Okura & Ansal, 2007)

For cyclic problems, such as the design of high-speed trains foundation, small strain stiffness is of crucial importance. It should not be ignored since it could lead to overestimation of deformations and under-design of structures. The former, is especially problematic in urban environments where deformations need to be within a certain range. The latter occurs by underestimating stresses and in the worst case scenario it can lead to collapse of infrastructure.

In order to predict this behavior, laboratory experiments such as cycling triaxial test, (oedemeter test), resonant column, seismic dilatometer, in-situ dilatometer and multi-channel analysis of surface waves (MASW) can be performed (Asslan, 2008). Alternatively it can be determined by empirical methods. These can only be utilized in cases

where they have been analyzed previously. Different empirical and laboratory methods and how different parameters is influencing can be found in (Wood & Dijkstra, 2015).

2.3 Railway-induced vibrations

2.3.1 Vibration generation mechanisms

The vibration generation mechanisms from rail traffic are usually categorized into two: the dynamic axle loading which is due joints of the tracks, unevenness of the wheel or track etc., and the quasi-static load which is the weight of the train imposed on tracks. In urban rail traffics, when the speed of train is not very high, the dynamic axle loading mechanism is dominant in ground vibration problems. But in terms of high-speed trains running on soft soil conditions, the quasi-static loading mechanism can be dominant and lead to severe track vertical deformations. This phenomenon is usually referred to as the superseismic motion, in comparison to the supersonic phenomenon in aeroacoustics.

Ground vibrations caused by rail traffics are generally a low frequency problem. Typical urban ground-borne vibrations are prominent in the frequency range from 40 to 80 Hz (Heckl et al. 1996). In terms of the affection to buildings, mechanical vibrations usually occur at 1 - 80 Hz, while at 16 - 250 Hz, the vibrations can re-radiate into rooms as structure-borne noise (Lombaert et al. 2000).

Measurements of ground vibrations induced by trains in Sweden (Suhairy, 2000) show that for high speed trains, the vibrational energy falls between 2 - 100 Hz.

2.3.2 The superseismic motion

The term 'superseismic' is an analogy from 'supersonic'. When an object on ground moves with a speed greater than the wave speed in the ground, the superseismic phenomenon can happen (Krylov, 2001). In the case of high speed train, as the train speed approaches the velocities of wave propagations in the ground, the vibration amplitude of the track will experience a dramatic increase; also an upward movement of the track can be observed. That is to say, the wave speed in the ground set a threshold of the train speed above which the induced vibration can be very harmful.

The superseismic phenomenon has be reported by Krylov (2001) theoretically, and by Kaynia et al. (2000) experimentally.

2.3.3 Vibration propagation in ground

The vibrations induced by railway traffic, constructions etc. can propagate through long distances in the ground, causing annoyance in residential areas. Vibrations propagate in the form of waves. And there are two major types of waves in an semi-infinite medium such as the ground: body wave and surface wave. Body waves include P-waves, or compressional waves, in which the particle movement is parallel to the direction of the propagating

wave; and S-waves, or shear waves, in which the particle movement is perpendicular to the wave propagation direction.

Surface waves can be observed at the surface of the medium, or at boundaries separating different layers. Rayleigh waves and Love waves are the two most common types of surface waves. Rayleigh waves are a more general type of surface wave, which can be excited in all kinds of half-space medium, while Love waves are an interferential wave, caused by interaction of incident and reflected waves in a layered medium (Kaufman & Levshin 2005, p.259).

Body waves and surface waves propagate in different manners. Assuming a point excitation is impinged on top of an isotropic homogeneous ground, both body waves and surface waves are generated. Body waves propagate homogeneously from the excitation point towards all directions, with their amplitude decreasing inversely proportional to distance. Surface wave, as is described by its name, propagates mostly along the surface; it's amplitude quickly disappeares in depth after one wavelength, but it's amplitude drop inversely proportional to the square root of distance. This means that the geometrical attenuation of the surface wave is slower than that of body waves. In fact, on the surface of the ground far away from the excitation source, most vibrational energy appear as Rayleigh waves (the dominating surface wave), roughly 67 % according to study, 26 % of the energy comes from shear wave, and 7 % goes into P-wave (Gutowski & Dym 1976).

2.3.4 Governing equations in ground vibration propagation

Under the assumption that the ground is a homogeneous and isotropic elastic material, with a continuous and small displacement distribution $\mathbf{u}(x, y, z)$, the ground vibration can be described with Navier's equation of motion:

$$\mu\nabla^2\mathbf{u}(x,y,z) + (\mu+\lambda)\nabla(\nabla\mathbf{u}(x,y,z))) + \rho\omega^2\mathbf{u}(x,y,z) = 0 \tag{2.5}$$

Here ∇^2 is the Laplacian operator, ∇ is the Nabla operator, μ and λ are the Lamé parameters of the ground, ρ is the density of the ground, ω is the angular frequency, and x, y, z are spatial coordinates. The equation is written in frequency domain.

Solving the equation with no adjacent boundary restrictions gives two wave motions: the P-wave and the S-wave. Their propagation velocities are given as follows:

$$c_p = \sqrt{\frac{\lambda+2\mu}{\rho}}, \quad c_s = \sqrt{\frac{\mu}{\rho}} \tag{2.6}$$

The solution of this equation can be found in different literatures, e.g. see Appendix B in Grau (2015a).

When equation 2.5 is solved with a bounding surface, e.g. a free surface, a solution for a surface wave motion can be found. This surface wave is known as the Rayleigh wave. The velocity of the Rayleigh wave c_r is dependent on c_s and μ:

$$c_r = \frac{0.87+1.12\mu}{1+\mu}c_s \tag{2.7}$$

Detailed information for this solution can be found in (Sadd, 1990). The solution shows that the Rayleigh wave velocity is independent of frequency, and the amplitude of Rayleigh wave decreases with the distance to the free surface (see Figure 2.10).

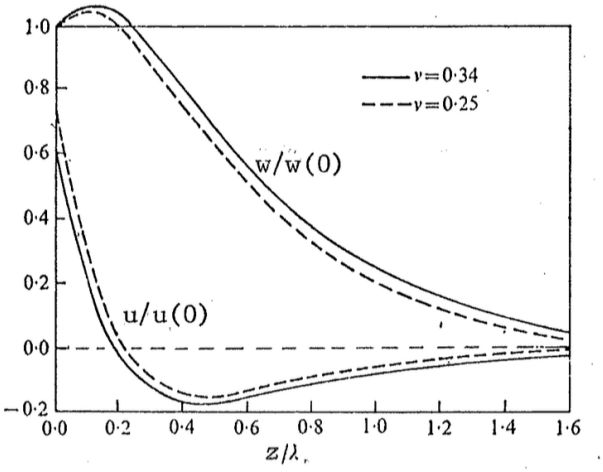

Figure 2.10: The vertical and horizontal amplitude of Rayleigh wave vs depth and Poisson's ratio (Sadd, 1990)

2.3.5 Literature study on theories for ground - structure interactions

Extensive research on the problem of foundation vibration on ground has been conducted since 1960s. The foundation to this problem was the theory of wave propagation in an elastic half space, first published by Lamb (1904). A detailed review of the earlier work can be found in (Richart et al. 1970) and (Gazetas 1983).

Earlier theoretical works aimed at describing and solving the problem with a set of ratio factors, regardless of their material properties. Gucunski and Peek (1993) presented an analytical solution of a circular disk on layered half-space. They assumed that the soil reaction distribution follows a ring method, and used a stiffness matrix for layered soil and for a circular plate to combine the motion of the two components.

Lysmer (1965) proposed that the 'foundation resting on soil' problem can be resembled as a single-degree-of-freedom 'mass-spring-dashpot' oscillator. Based on this, Baidya el al. (2006) developed a Mass-Spring-Dashpot model to calculate the resonance of concrete foundation on layered soil underlain by a rigid boundary, where he introduced ways to find equivalent stiffness for layered soil. Experimental results can be found in (Baidya & Krishna 2001).

Grau (2015a) presented an analytical solution of a rectangular concrete plate resting on layered soil, where he focuses more on the modal coupling between the plate and the ground. He made an analogy between the ground vibration from the foundation and sound radiation from a vibrating plate, and showed that the imaginary part of the ground impedance works as either add-stiffness or add-mass effect to the plate, depending on its sign.

2.4 Finite element modelling

Finite element (FE) method has become a very well established as the main tool for engineering analysis. It intends to solve differential equations that describes the static / dynamic behavior of a complicated object.

The key idea is to discretize the complicated geometry into small, simply-shaped elements (such as triangle or polygon). Each element can be treated as a complete physical system, and the equation system that describes a single element is easy to solve. Then, different elements are connected through their common nodes, where they have the same displacement. Last, at the very boundaries of the whole geometry, displacement (or velocities or restrains) of those nodes should be clearly given, which then leads to a unique solution to the whole system.

There are several factors that can affect the accuracy of the FE modeling, for example, the mesh size and quality of the meshes, boundary conditions, shape functions, etc.,which need to be treated carefully.

Chapter 3

Long-term settlement prediction

As mentioned in the background, the maximum settlement which is allowed by Trafikverket for the railway foundation is 30 mm after 120 years. The constitutive models used for the prediction of the long-term deformation were the Creep-SCLAY1S model for the soil and Mohr's Coulomb model for the embankment and the subgrade body. Plane strain condition is used with open hydraulic boundaries in the sides, except for the X_{min} and X_{max} boundaries. Since the geometry of the railway foundation is symmetric, only one side of it was considered. The phreatic level is assumed to be situated at 2 m beneath the ground level.

3.1 Constitutive model

The model Creep-SCLAY1 was developed by Sivasithsmparam, Karstunen and Bonnier. It is a model used in PLAXIS 2D where the creep behaviour of anisotropic clay can be determined. Before, the S-CLAY1S model was used. However, there were problems related with rate-dependency and underestimation of time dependant settlements. These problems are overcome with the Creep-SCLAY1S model. It is essential to take into account the strain rate even for undrained soils; since creep is a time dependant deformation and it increases gradually. One of the main assumptions of the model is that an entirely elastic domain does not exist (Sivasithamparam, Karstunen, & Bonnier, 2015).

The parameters used in the Creep-SCLAY1S model are based on laboratory tests. Of the parameters used, five of them are similar to the Modified CAM-CLAY model. The remaining ones are similar to the Isotropic parameters from the S-CLAY1 model and the Viscosity parameter which used on the Soft soil creep model.

3.2 Model parameters

Due to limited time, the parameters used in this model are based on a research project on energy pile which was conducted in the outskirts of Gothenburg. The samples were taken from a 6-10 m deep homogenous deposit clay with high plasticity index. These were tested in a laboratory and the results were presented in the research paper "Comparison

of the performance of mini-block and piston sampling in high plasticity clay" Karlsson, Bergström and Dijkstra 2015. Since the parameters from this research were used on the Mac-s model, the parameters were reanalysed for adapting them to the Creep-SCLAY1S.

In the FE-model, the clay was divided into three layers and there is a fourth layer for the subgrade body. Thereafter, this was input to the Creep-SCLAY1S model assuming undrained behaviour, type A. The embankment was divided into two parts and the Mohr's Coulomb model with drained behaviour was used. The parameters used to predict the long settlement are presented in Table 3.2 for the clay and for the embakment at Table 3.1. The subgrade body and the bottom part of the embankment contains filler to improve the soil condition. The top part of the embankment was built with crushed stone and the concrete base is composed of sand, cement and asphalt (Fang & Cerdas, 2015).

Material	$\boldsymbol{\rho}(kg/m^3)$	**E** (MPa)	$\boldsymbol{\nu}(-)$	$\boldsymbol{\eta}(-)$	$\boldsymbol{h(m)}$
Track slab	2450	$35 * 10^3$	0.3	0.04	0.21
Concrete base	2300	$33 * 10^3$	0.167	0.04	0.14
Embankment	2200	25	0.25	0.06	3
Dry crust	1800	7	0.30	0.06	2

Table 3.1: Material parameters for the railway foundation

Depth (m)	$\boldsymbol{\rho}$ (kg/m^3)	$\boldsymbol{\nu_{ur}}$ (-)	$\boldsymbol{\lambda^*}$ (-)	$\boldsymbol{\mu^*}$ (-)	$\boldsymbol{\chi_0}$ (-)	$\boldsymbol{\omega}$ (-)	$\boldsymbol{\omega_d}$ (-)	$\boldsymbol{\tau}$ (day)	$\boldsymbol{\xi}$ $(-)$	$\boldsymbol{\xi_d}$ (-)	$\boldsymbol{M_c}$ (-)	$\boldsymbol{M_e}$ (-)	$\boldsymbol{\kappa^*}$ (-)	$\boldsymbol{\alpha_0}$ (-)	$\boldsymbol{OCR}$ $(-)$
$2-5$	1600	0.2	0.097	$1.25e^{-3}$	8.0	200	0.852	1	8.5	0.2	1.6	1.1	0.015	0.491	1.45
$5-25$	1600	0.2	0.097	$1.25e^{-3}$	8.0	200	0.852	1	8.5	0.2	1.6	1.1	0.015	0.491	1.50
$25-40$	1600	0.2	0.097	$1.25e^{-3}$	8.0	200	0.852	1	8.5	0.2	1.6	1.1	0.015	0.491	1.60

Table 3.2: Material parameters for the Creep-SCLAY1S model

3.3 Geometry and mesh

The railway foundation according to Trafikverket is a 3 m embankment which comprises 2.7 m lower subgrade. The embankment is underlaid by a 0.7 m subgrade, see Figure 3.1. Above the embankment, there is a concrete base 6.8 m long. On the concrete base, the 2.4 m wide railway track slab is situated.

For avoiding the boundary effects on the material velocity on the PLAXIS model, a dimension of 40*100 m was used for the soil. The soil is divided into 4 layers, the upper three layers consisting of clay and the lower one is a subgrade body which improves the soil properties. The clay layers have a high plasticity index and are 5, 25 and 40 m deep respectively. The subgrade body is 2 m deep.

Due to the large dimensions of the geometry, the mesh size distribution is divided into sections depending on the vertical displacement. The settlement is largest beneath the embankment, therefore the mesh size in that area is finer, in this way the model is optimized, see Figure 3.2. 4547 6-noded elements mesh size are generated.

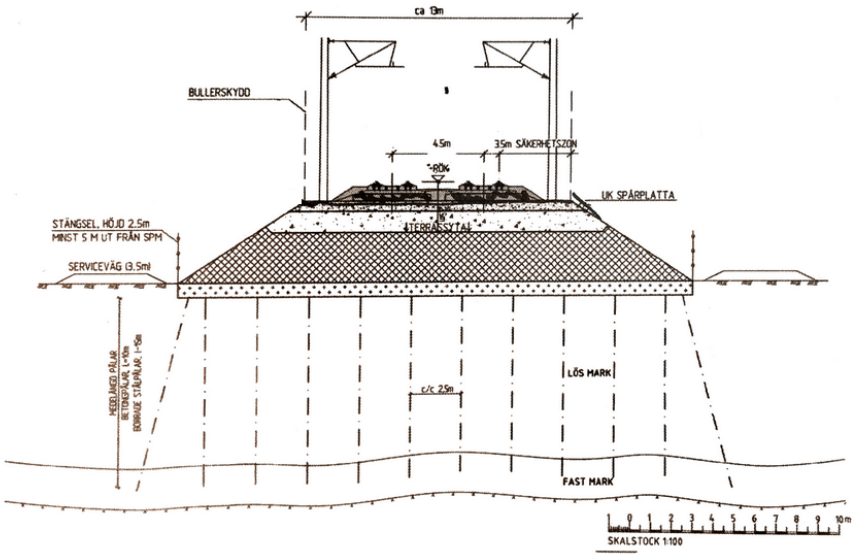

Figure 3.1: Railway foundation presented by Trafikverket

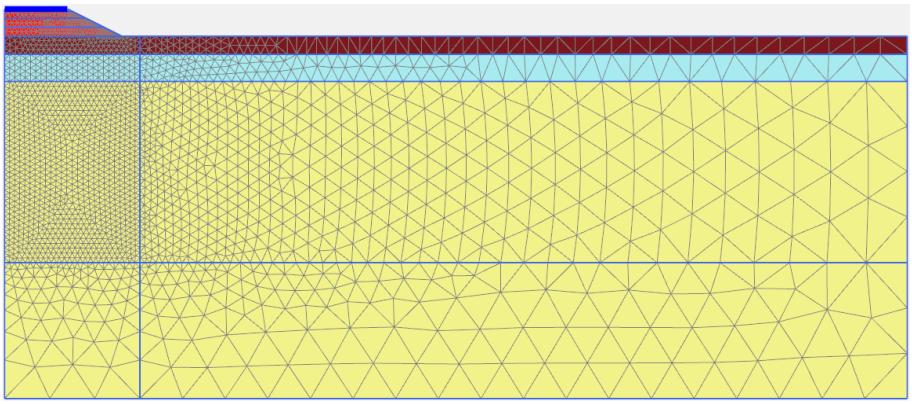

Figure 3.2: Mesh size and soil layers

3.4 Vertical displacement analysis

The results from the long term simulation determines that the vertical displacement after 120 years is approximately 1.2 m. This is for the condition that two static axle loads of 17 tons are permanently applied on the track slab. This assumption is very conservative since trains will affect the soil as a moving load during a certain time and it is expected that there will be up to 10 train passages per hour according to Trafikverket. In Figure 3.3 , the vertical displacement with respect to time is shown. As it can be seen, the settlements without axle loads are approximately 60% less than with axle loads. The requirement according to Trafikverket is that the settlement after 120 years should be less than 30 mm which is very small in comparison with the results of this simulation. The settlement prediction were simulated without any soil improvement method, such as pile system, lime columns, stone columns, etc.

Given that there were large deformations, updated lagrangian approach and updated pore water pressures were applied in the model to obtain more accurate deformation predictions. Utilizing updated lagrangian approach leads to geometry changes which are accounted for in the second order deformation effect. Large deformations lead to a reduction in effective overburden with time, in order to take this into consideration, updated pore water pressure was utilized (Brinkgreve, Kumarswamy, & Swolfs, 2016).

In the following sections, a deeper analysis of the dynamic response of the soil will be performed for analyzing the long term settlement under a dynamic load where this PLAXIS model will be combined with a COMSOL Multiphysics model.

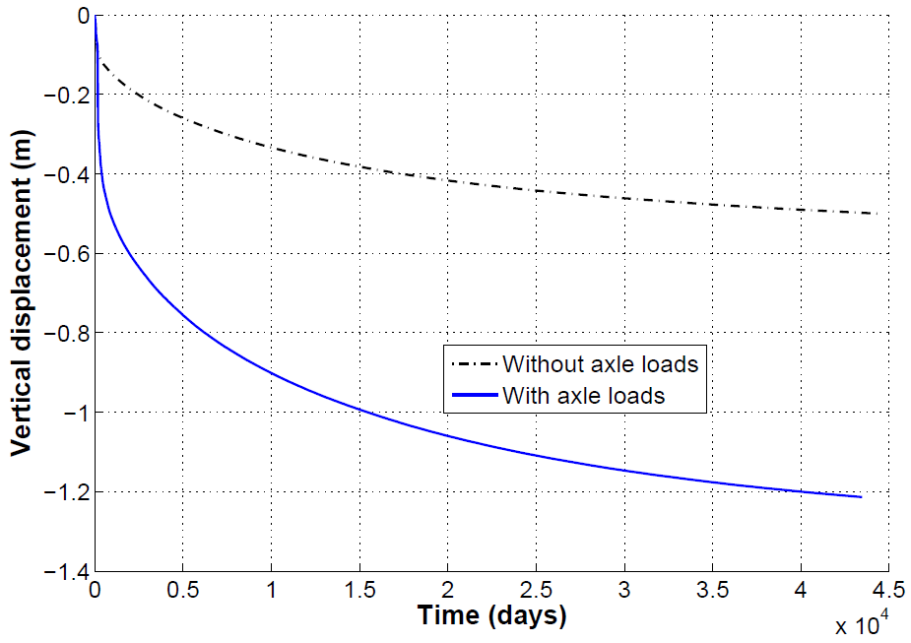

Figure 3.3: Vertical displacement with and without a applied static axle loads

3.5 Stability analysis

In the construction of an embankment, it is important to take into account the stability during its service life. To increase the stability, the staged construction method is used. This method is used on soft sensitive soils with low shear strength and high compressibility. It is recommended to construct each stage in the shortest construction time possible. Before the next stage can commence, the safety factor should be adequate. The safety factor is defined as the ratio between the maximum available shear strength and the needed shear strength for equilibrium.

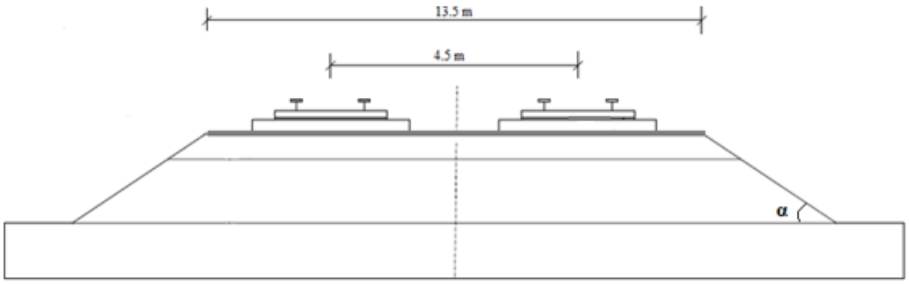

Figure 3.4: Railway foundation used in the model

The angle, α of the embankment, which was recommended by Trafikverket was reduced from 33.7° to 26.6° in order to increase the stability. The friction angle for the Mohr's Coulomb model in the embankment was determined to be 40°. The bottom and top layers of the embankment were built in four stages, with a time step of 30 days between the stages. The concrete base and the track slab were built with a time step of 15 days. As mentioned in the previous chapter, a deep analysis of the stability of the embankment was not carried out so the time step was not analyzed in detail. In further research, it is recommended to study the stability of the embakment under cyclic loading.

3.6 Model parameters sensitivity

As mentioned in the previous section, the Creep SCLAY1 model was utilized in the constitutive model where the isotropic (λ^*, κ^*), anisotropic (α_0) and viscous parameters (μ^*) are used. In figures 3.5, 3.6, 3.7, the sensitivity of those parameters and of the overconsolidation ratio were analyzed by considering an upper and lower bound. These were increased and decreased, respectively, by 30% of the initial values, see Table 3.2.

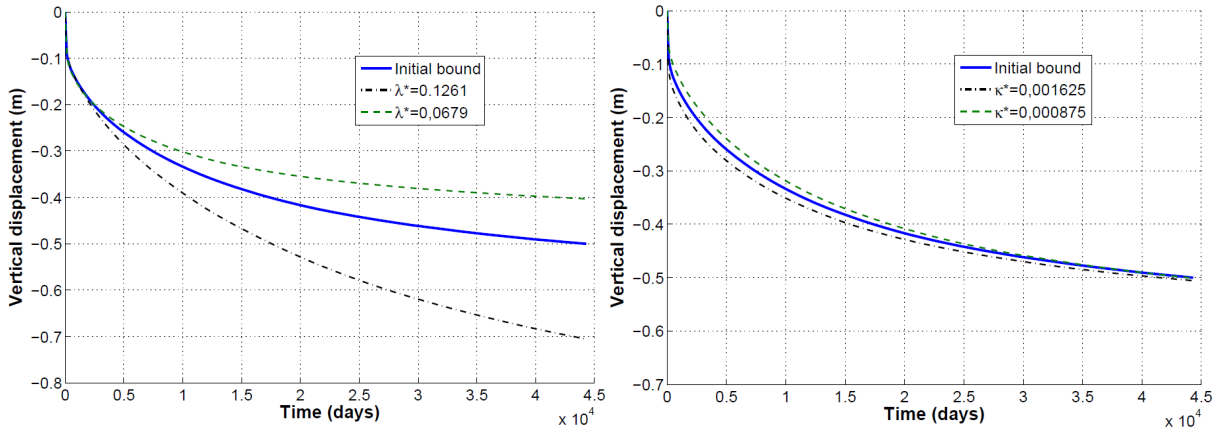

Figure 3.5: Sensitivity of the isotropic parameters

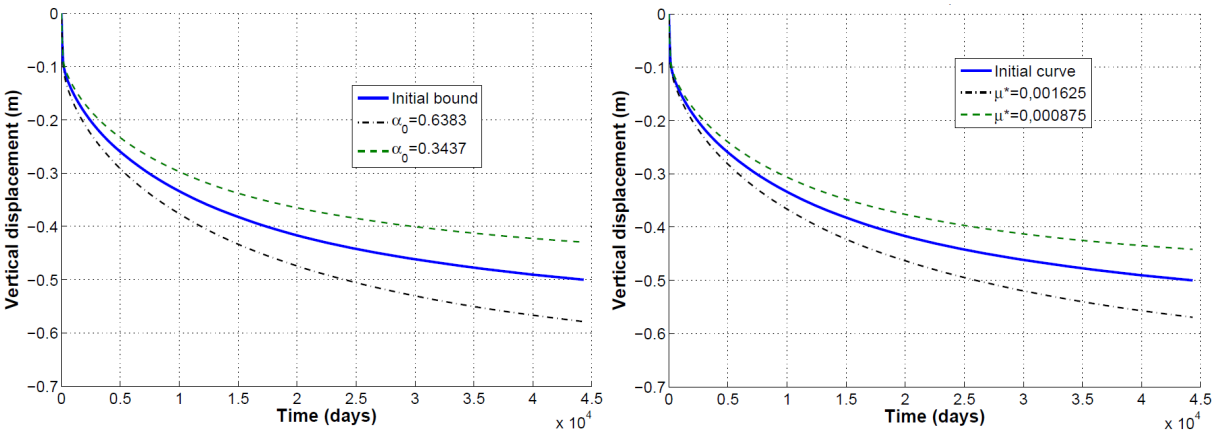

Figure 3.6: Sensitivity of the anistropic and the viscous parameter

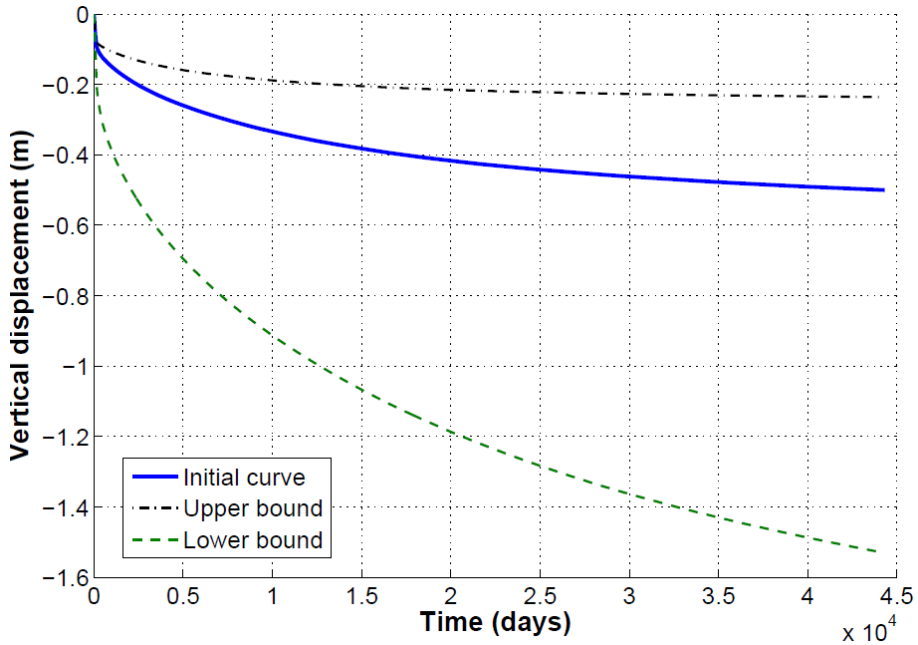

Figure 3.7: Sensitivity of the overconsolidation ratio.

3.6.1 Overconsolidation ratio

It was determined that the overconsolidation ratio is the most sensitive parameter and therefore has a significant influence on the vertical displacement. The creep strain rate was obtained from Equation 3.1, where $\dot{\Lambda}$ is the visco-plastic multiplier, see Equation 3.2. As it can be seen, the overconsolidation ratio is the most critical parameter. A decrease in the overconsolidation ratio leads an increase in the visco-plastic multiplier which results in an increase of the creep strain rate.

$$\dot{\epsilon_v} = \dot{\Lambda}\frac{\partial p'_{eq}}{\partial p'} \tag{3.1}$$

$$\dot{\Lambda} = \frac{\mu^*}{\pi}\left(\frac{1}{OCR}\right)^{\beta}\left(\frac{M^2 - \alpha^2_{Ko^{NC}}}{M^2 - \eta^2_{Ko^{NC}}}\right) \tag{3.2}$$

3.6.2 Viscous behavior

Soil which is subjected to periodic loading and unloading exhibits a gradual deformation and recovery. The rate depends on the frequency of the dynamic loading, the duration of the load and the behavior of the soil. For the latter, viscous behavior of the clay was analyzed. This was chosen as it is a governing parameter for the creep behavior under dynamic loading. The clay was assumed to be homogenous.

Viscosity can be determined by analyzing volumetric strain versus time or through the secondary compression index which can be obtained in void ratio versus time.

By performing a sensitivity analysis on this parameter, it was determined to have a significant impact on the vertical displacement. Firstly, the parameter was increased and decreased by 30% which did not result in a large variation. However, when the parameter was multiplied by ±10 times there was a significant impact on the result, see Figure 3.8.

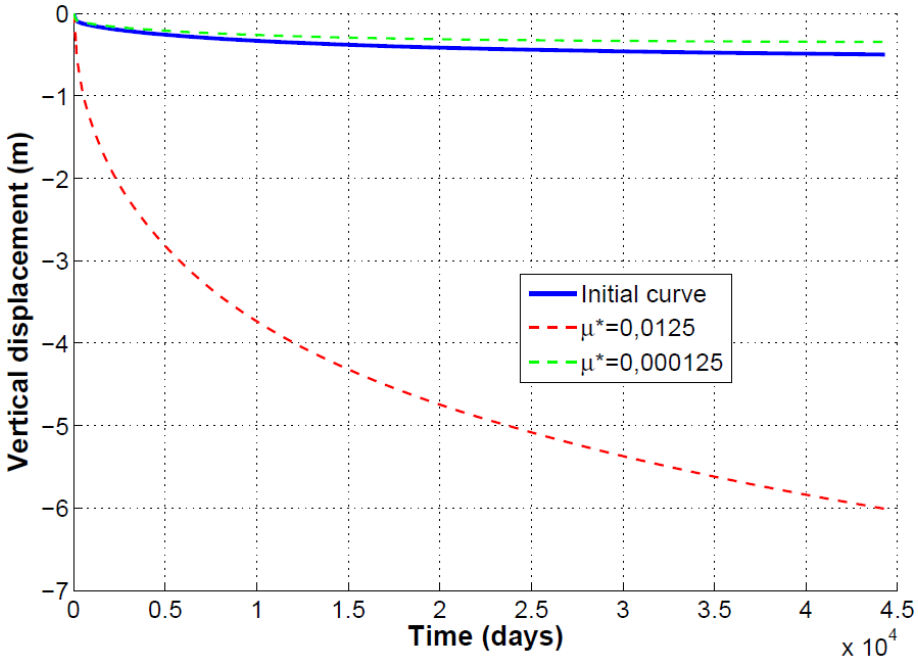

Figure 3.8: Sensitivity of the viscous parameter

3.6.3 Phreatic level

Changes in phreatic level results in a variation of vertical displacement, a decrease would lead to larger vertical displacement and vice versa. Since the chosen phreatic level is an assumption, a variation of the vertical displacement versus the time is presented for different phreatic levels, see Figure 3.9. As can be seen, there is a considerable difference in the vertical displacement for different phreatic levels. Therefore, it is recommended to investigate which is the phreatic level which should be used. The changes in phreatic level depends on a number of heterogenic and dynamic factors, such as human activities, climate changes, weather, loading frequency, infiltration etcetera.

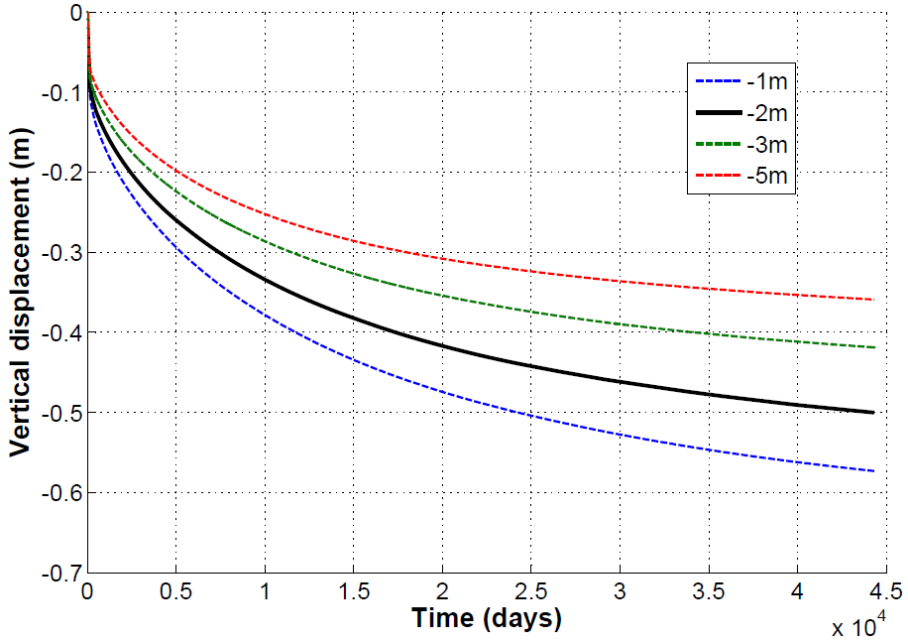

Figure 3.9: Changes in phreatic level

Chapter 4

The dynamic validation model

In order to (1) gain some insight into the dynamic response of the concrete slab, and (2) validate the dynamic model with respect to its mesh size, geometry set-up and boundary condition, a FE model of a rectangular concrete slab resting on a two-layered ground is created in the commercial FE modeling software *Comsol Multiphysics 5.1*. The concrete slab is subject to an unified impact force (1 N).

The analytical solution of this simplified situation is provided by Grau et al. (2015b), using an analogy impedance method. The geometry and material parameters of this model is chosen in accordance with Grau's doctoral thesis (Grau 2015b).

4.1 Implementation of the model

4.1.1 Geometry

Figure 4.1 (right) shows the geometry of the model from Comsol, where a concrete slab is lying on a two-layered ground. The size of the concrete slab is $6.6 \times 28 \times 0.4\ m^3$; the thickness of the top soil layer is 5 m, and the bottom layer is extended to infinity. The ground is modelled as a quarter of a sphere with a radius of 30 m, which is divided into two parts to represent the two soil layers.

Figure 4.1 (left) shows the layout of the loading and measurement positions on the concrete slab and on the soil surface. These positions are used in Grau's measurement (Grau 2015b), and therefore used in the comsol model to compare the results. A unified impact load (1 N) is applied at the center of the slab, 1.65 m away from the edge. The acceleration is measured at 5 positions along the central line, one on top of the concrete slab and 4 on the ground.

Due to the symmetry of the total geometry, the Comsol model is only built for half of it. Therefore in Figure 4.1, the picture to the right represents half of the geometry shown in the left picture.

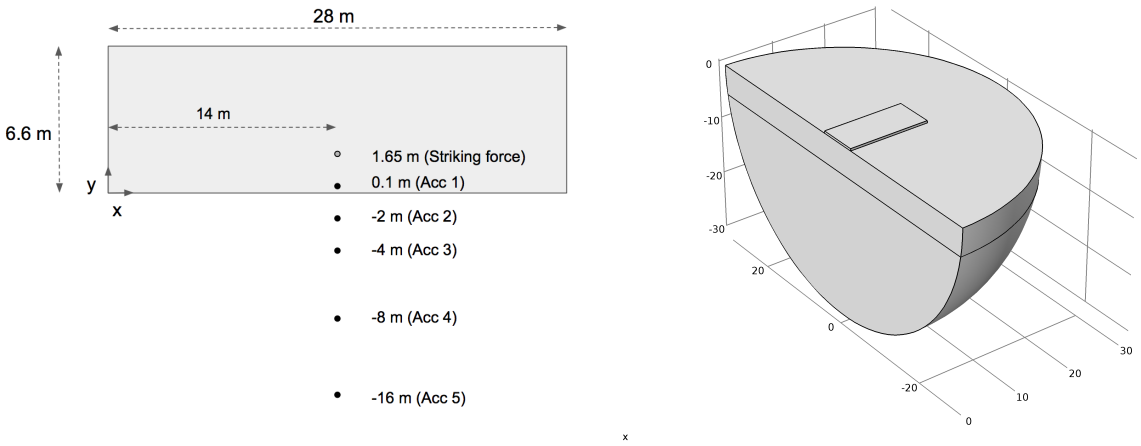

Figure 4.1: Geometry and measurement positions of the FE model

4.1.2 Material properties

The concrete slab has the following characters: $\rho = 2500\ kg/m^3$, $E = 2.5 \times 10^{10}\ Pa$, poisson's ratio $\mu = 0.3$, and an isotropic loss factor $\eta = 0.05$. The soil properties are described with its p-wave and s-waves velocities and isotropic loss factors:

-	$\rho(kg/m^3)$	$C_p\ (m/s)$	$C_s\ (m/s)$	η
soil top	1500	1000	300	0.06
soil bottom	1500	2000	900	0.06

Table 4.1: Material properties of the soil

4.1.3 Physics & boundary conditions

The 'Linear Elastic Material' physics in the Solid Mechanics module is applied to both the concrete slab and the soil layers.

A **low-reflecting boundary** condition is applied at the outer surface of the soil, which is marked in purple in Figure 4.2 left. The low-reflecting boundary applies the following equations:

$$\sigma \mathbf{n} = -j\omega \mathbf{u} \mathbf{d}; \quad d_i = 0.5\rho(c_s + c_p),\ i = 1, 2, 3 \tag{4.1}$$

where σ is the stress, $\mathbf{n}$ is a unit vector representing the normal direction of the chosen surface, $\mathbf{u}$ is the displacement vector, and $\mathbf{d} = (d_1,\ d_2,\ d_3)^T$ is the impedance of wave propagation. This equation shows that the low-reflecting boundary condition applies an isotropical impedance that is the average of the S-wave impedance and the P-wave impedance. The intension is to match the impedance at the boundary with the wave propagation impedance, so that there will be no reflections at this boundary. However since Comsol cannot separate the displacement field of P-wave from that of S-wave, it is a compromise to apply the average of the impedance of the two wave types. Investigations have been done with $d_i = \rho c_p$ or $d_i = \rho c_s$, but no major effects to the response of the concrete slab have been seen.

Figure 4.2: Boundary conditions, left: low-reflecting boundary, right: symmetric boundary

A **symmetry constraint** is applied at the cross section, marked in purple in Figure 4.2 right. It applies the following equation to the chosen surface:

$$\mathbf{n} \cdot \mathbf{u} = 0 \tag{4.2}$$

where $\mathbf{n}$ and $\mathbf{u}$ are the same as in Equation 4.1. This constraint sets the displacement within the surface to be free, while the displacement in the out-of-plane direction is zero. Hence the system is symmetrical alone the chosen plane or surface.

No constraints are applied for the rest of the boundaries.

4.1.4 Mesh

In order to balance the number of meshes and computation time, the mesh of the model is user-defined so that it is finer on or near the concrete slab, and coarser at the outer boundary of the geometry, as shown in Figure 4.3. In order to increase the mesh precision below the concrete slab, a $3 \times 14 \times 14m^3$ mesh-control region is defined, where the mesh size is chosen to be 'extra fine'.

The mesh type is 'free tetrahedral' for all domains. The mesh order (or the discretization order) is quadratic, which means there exists one intermediate node at each edge of the tetrahedral mesh element. Comsol Multiphysics choose the discretization order to optimize solving different types of partial differential equations. In solid mechanics, the default discretization order is quadratic.

The averaged mesh size and quality of the model are listed in Table 4.2. Mesh quality is an index between 0 and 1, and the closer it is to 1, the better the mesh quality. In general, a mesh quality of above 0.1 is deemed as good enough (Griesmer 2014).

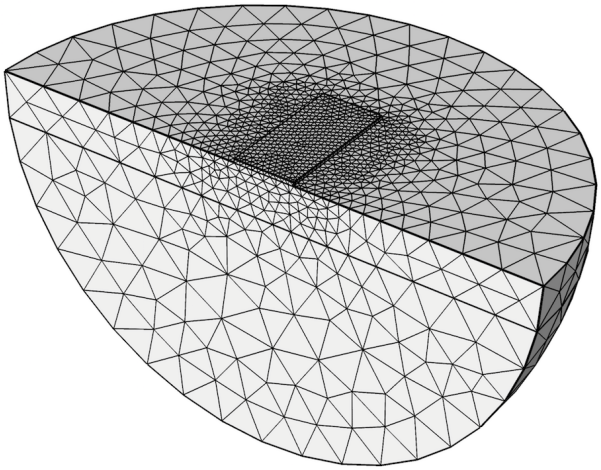

Figure 4.3: User-defined mesh

Material	**Avg. mesh size** (m)	**Avg. mesh volume** (m^3)	**Avg. mesh quality**
Concrete slab	0.74	0.024	0.72
Top soil layer	3.67	3.67	0.74
Bottom soil layer	4.89	7.13	0.76

Table 4.2: Parameter of the user-defined mesh

As a rule of thumb in finite element method, the mesh size should be at least 1/6 of the wavelength in order to provide valid results for this frequency. With quadratic elements, however, with an intermediate node at their edge, the mesh size can be 1/3 of the upper frequency wavelength.

In the concrete slab, an average mesh size of 0.74 m gives an upper frequency limit of 244 Hz. In the soil, within 2 m away from the concrete slab, the element size is below 1.01 m, which yields an upper frequency limit of 354 Hz for p-wave, and 100 Hz for s-waves; within 14 m away from the center of geometry, the averaged element size is 2 m, which gives an upper frequency limit of 166 Hz for p-wave, and 50 Hz for s-waves.

This means that the results of the FE model is valid up to 244 Hz for the concrete slab, 100 Hz for position 2 and 3, and 50 Hz for position 4 and 5.

4.2 Mesh convergence study

The influence of the mesh size on the calculated results is studied. Figure 4.4 shows the transfer inertance on position 1 for 10, 20, 40 and 100 Hz, calculated with different mesh size.

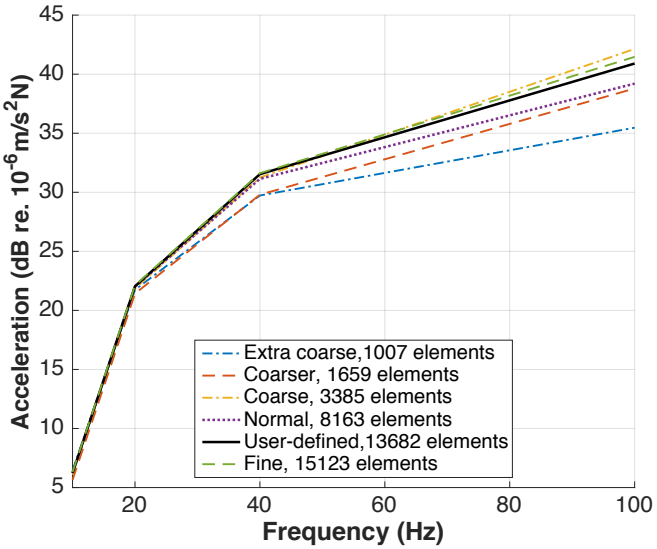

Figure 4.4: Dynamic response on position 1, different mesh size

As can be seen in Figure 4.4, a lower quality mesh generally results in an underestimated transfer inertance. The results at 40 Hz start to converge at a 'normal' mesh size. At 100 Hz, the results start to show a tendency of converging at the user-defined mesh size. It would be more convincing to calculate the 'finer' and 'extra fine' mesh size to validate the convergence behaviour, however due to the limited computation power, the calculation for a 'finer' and 'extra fine' mesh did not proceed. However, regarding the dynamic response of the concrete slab, it is convincing that the user-defined mesh provides a decent result that does not differ much from a even finer mesh.

4.3 Results

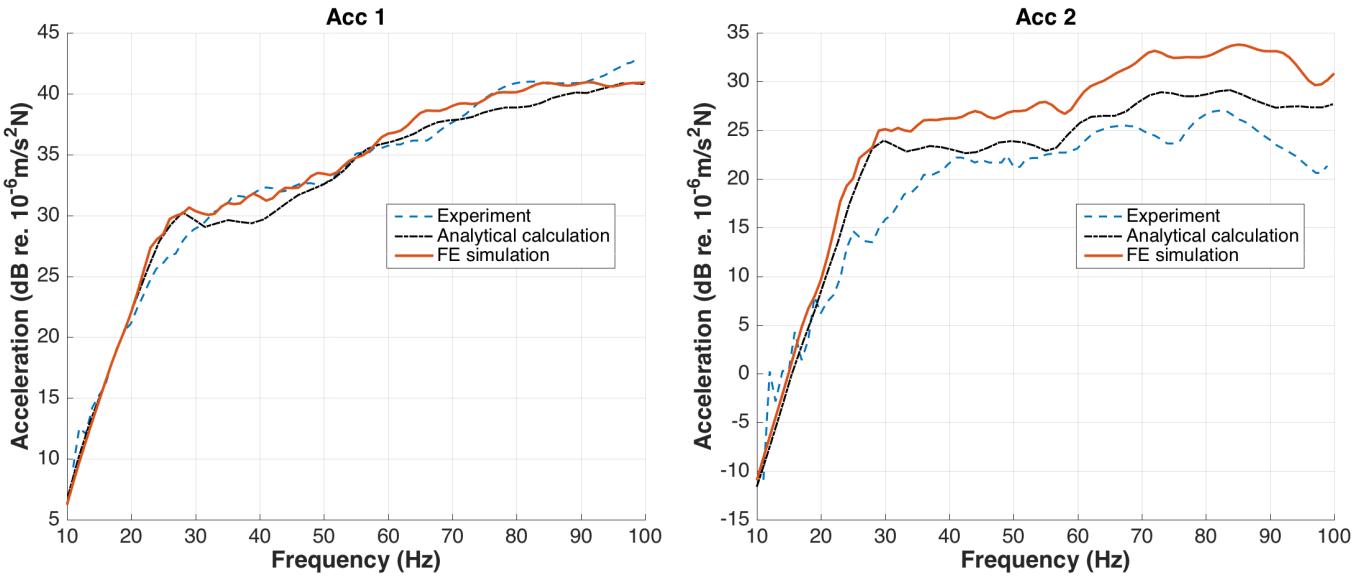

Figure 4.5: Transfer inertance at position 1 and 2

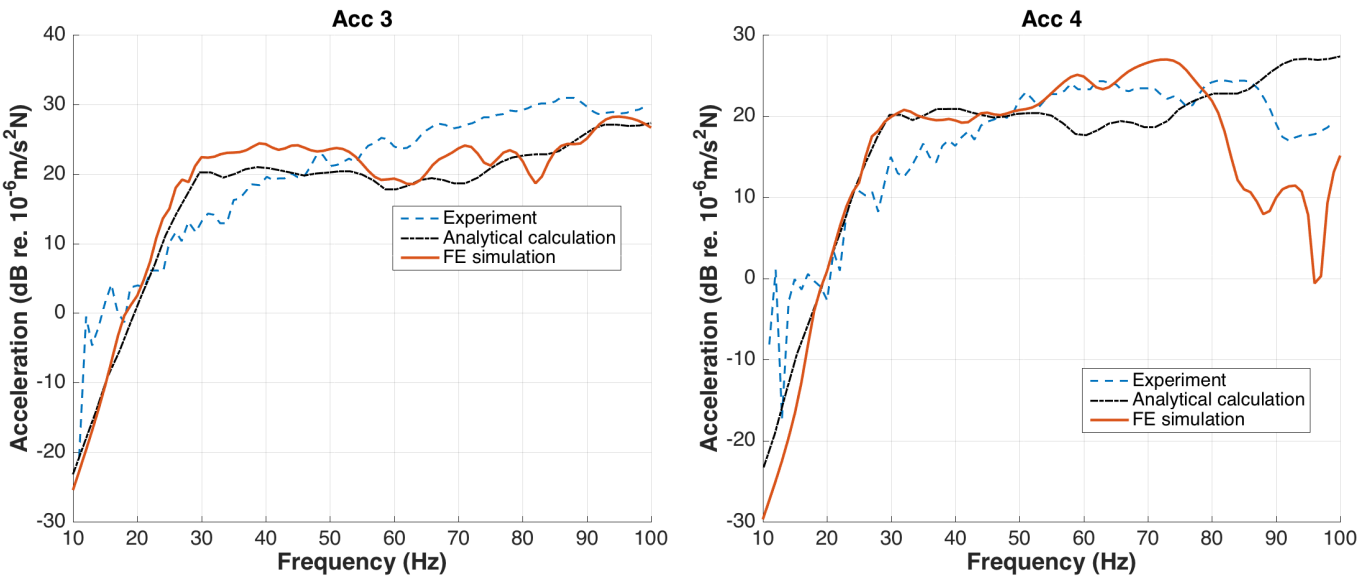

Figure 4.6: Transfer inertance at position 1 and 2

Figure 4.5 - 4.7 shows the acceleration on top of the concrete slab calculated from the Comsol model, compared with Grau's data. The result from position 1 - on the concrete slab agrees very well to the analytical solution, with a maximum deviation of approximately 3 dB. At position 2 - 5, a good agreement between the FE model and the analytical solution can be found at roughly 10 - 30 Hz; while they deviate in a bigger manner at higher frequencies. This can be attributed to that the mesh size in the soil domain is not small enough, which can only provide a solution valid up to 50 Hz.

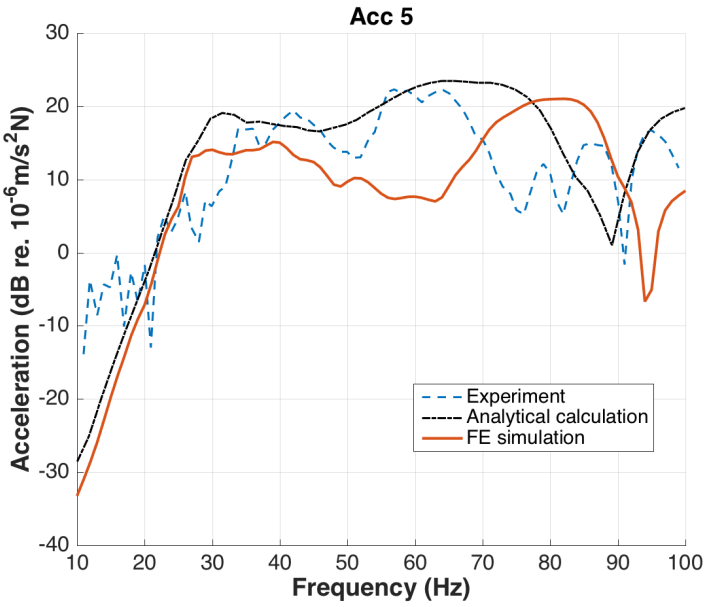

Figure 4.7: Transfer inertance at position 1

4.4 Influence of symmetry boundary conditions

Three geometry set-ups of the model are studied: a whole geometry, a halved one, and a quarter one, as shown in Figure 4.8. Low-reflecting boundary conditions are applied to the surface of the sphere for all three cases. Symmetry boundary condition is applied on the cross section of the halved geometry, and on two cross sections of the quarter geometry. An impact force of 1 N is applied at the center of the plate. A 'fine' mesh quality is chosen for all three geometries. The intension is to see if the geometry set-up has any influence on the calculated results.

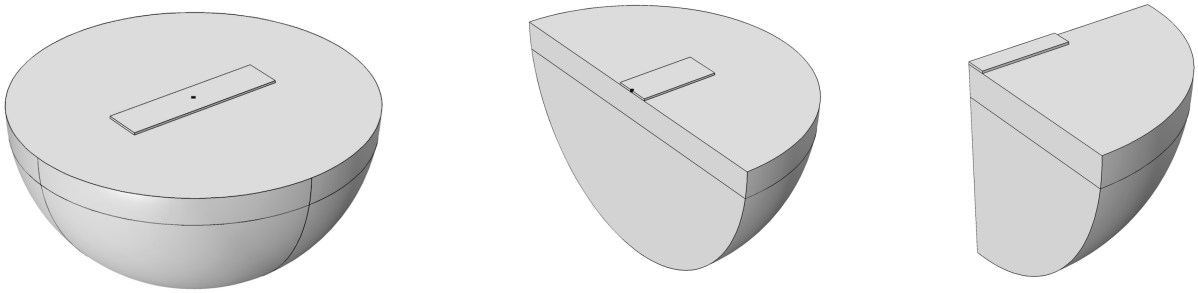

Figure 4.8: Three geometry set-ups

The transfer inertance for position 1 and 2 is calculated from the three geometry setups, and presented in Figure 4.9. As can be seen, using half or a quarter of the original geometry does have an effect on the inertance level: it rises by 6 dB when the geometry is halved. However, the shape of the transfer inertance against frequency does not change with the geometry. This is due to that the symmetric boundary applies the same load on the boundary to the other side of the domain, which leads to a 2 N impact force in total for the half geometry, and 4 N force for the 1/4 geometry, hence the 6 dB increase in levels. Therefore corrections of the result should be made regarding the geometry used, or simply apply a 0.5 N force for the half geometry and a 0.25 N for the quarter one.

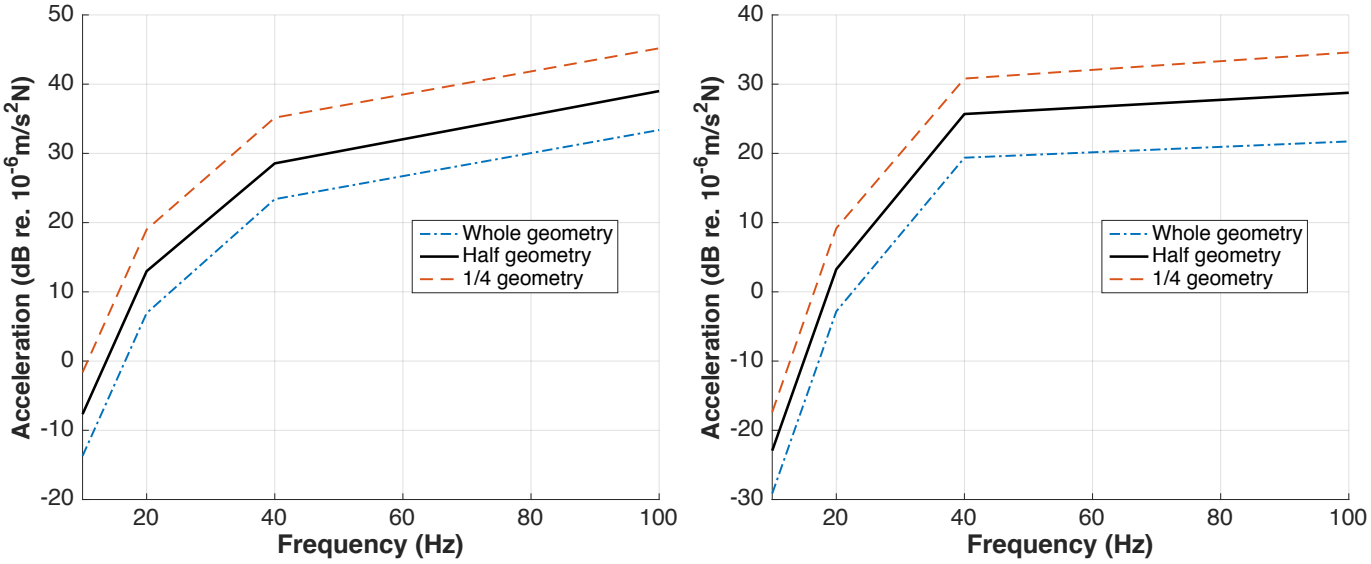

Figure 4.9: Dynamic response on position 1 (left) and position 2 (right), different geometry

4.5 Low-reflecting boundary condition study

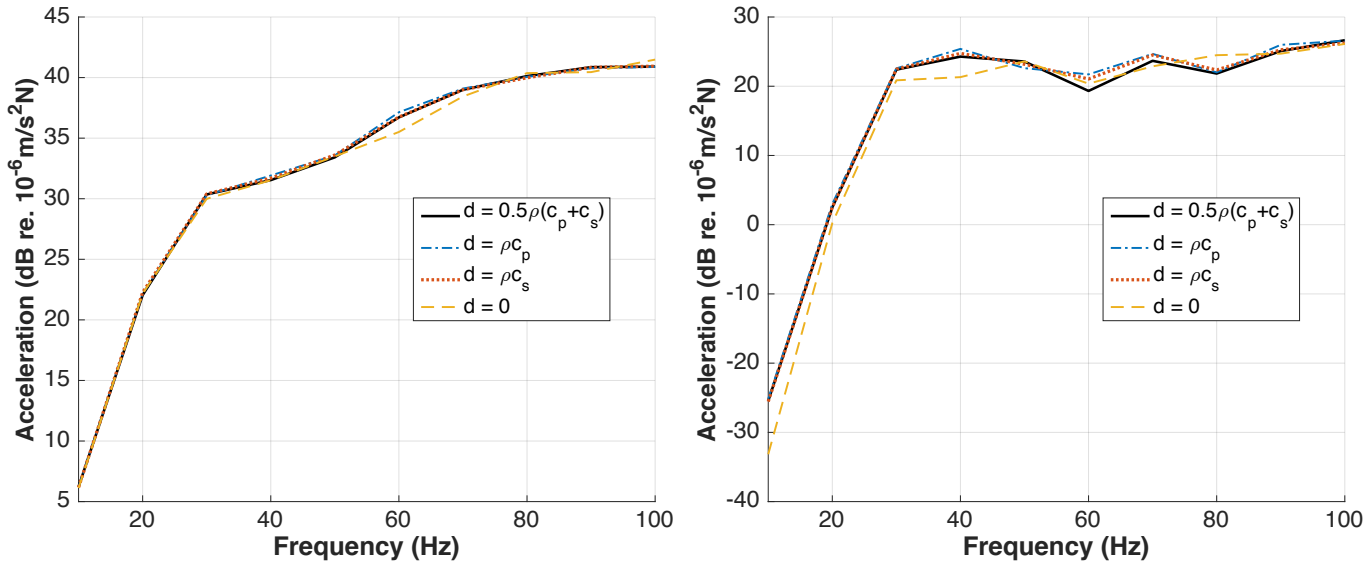

Figure 4.10: Dynamic response on position 1 (left) and position 3 (right), different low-reflecting boundary

In COMSOL Multiphysics, the low-reflecting boundary condition defines the mechanical impedance (d) at the boundary to be identical to the wave propagation impedance in order to absorb the incoming waves. The default impedance is $d = 0.5\rho(c_p + c_s)$, where c_p and c_s are the velocity of the p- and s-wave, which is used in the validation model. To further explore the influence of the low-reflecting boundary on the results, three other

impedances are applied: $d = \rho c_p, d = \rho c_s, d = 0$, representing that the boundary only absorbs p-wave, only absorbs s-waves, or has no absorption at all (which is the same as not appling this low-reflecting boundary condition). The corresponding transfer inertance at position 1 and position 3 under the 4 different low-reflecting boundaries are presented in Figure 4.10.

As can be seen in Figure 4.10 (left), at position 1, the transfer inertances of the 4 different cases have almost no difference at below 50 Hz; a 2 dB difference between the case of $d = 0$ and the others can be observed at 60 Hz. On the other hand, at position 3, $d = 0$ results in a minor reduction at below 50 Hz compared to the other cases. Between the cases of $d = \rho c_p$, $d = \rho c_s$ and $d = 0.5(\rho c_p + \rho c_s)$, the differences are generally very small.

This study shows that the low reflecting boundary condition applied at the edge of the geometry does not seem to have a distinct effect on the dynamic response on or at close to the concrete slab. This study is very preliminary, since it uses a frequency step of 10 Hz, and might have missed differences (resonance peaks) caused by different boundary conditions.

4.6 Size of the half-sphere

It is also of the author's intension to examine how the size of the half-sphere might affect the modelling results. Therefore another calculation has been done with a 60 m radius half-sphere to compare with the results presented in Chapter 4.3, see Figure 4.11.

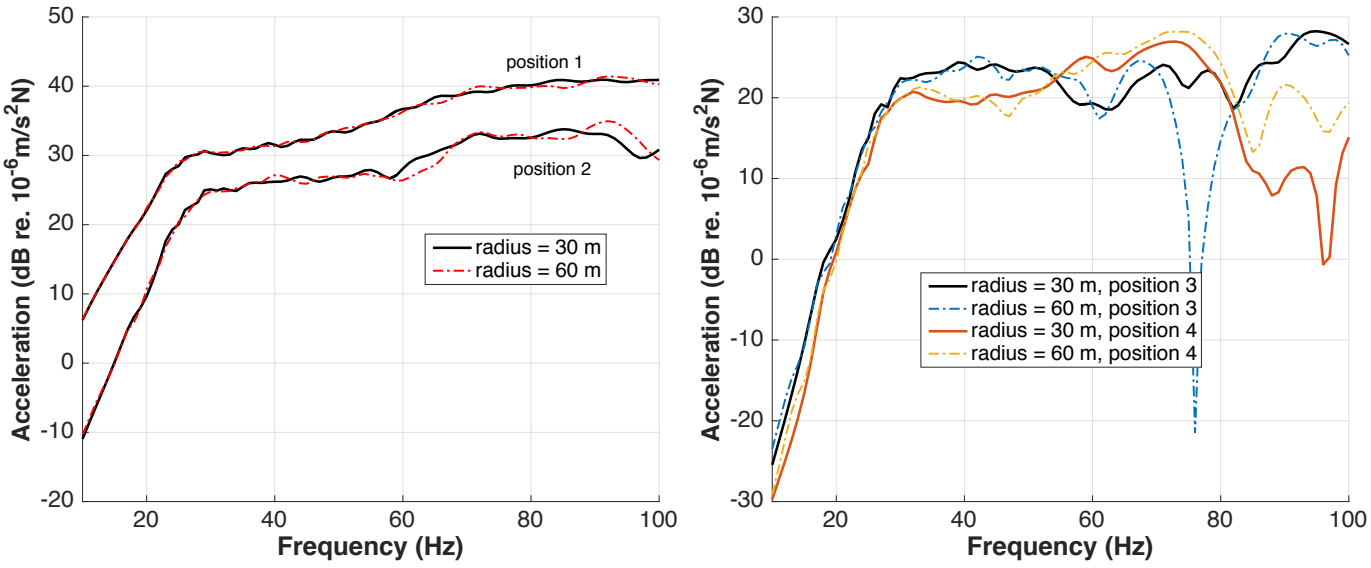

Figure 4.11: Transfer inertance at position 1 and 2 (left) and position 3 and 4 (right), with different size of the ground geometry

-	**Model with 30 m radius**	**Model with 60 m radius**
-	Avg. mesh size (m)	Avg. mesh size (m)
Concrete slab	0.74	1.20
Top soil layer	3.67	4.2
Bottom soil layer	4.89	8.99

Table 4.3: Mesh size of the two models

As can be seen, for position 1 and 2, the differences between the model of 30 m and 60 m radius are not very substantial. This can lead to a conclusion that the radius of 30 m is already big enough for obtaining a good result for the concrete slab and its adjacent area. For position 3 and 4, the results from the two models start to deviate at above 55 Hz. This deviation is more likely to be attributed to the difference in the mesh size of the two models, as listed in Table 4.3. It has been discussed in Chapter 4.1.4 that the results of higher frequencies are more sensitive to mesh size changes, since the applied mesh size does not fulfill 1/6 of the wavelength in soil.

Chapter 5

Determination of the dynamic response of the soil

In order to analyze the dynamic response of the soil with respect to long term soil degradation, a model simulating the dynamic response of the embankment using COMSOL Multiphysics and the static long term prediction model simulated by PLAXIS 2D need to be combined. In order to combine these models, a number of assumptions have been made due to limited access to regional field data.

5.1 Backbone curves

The stiffness degradation curve also known as the backbone curve is one of the optimal ways to represent the behavior of soft soil under dynamic load. It can be utilized to study the dynamic instability, the damping ratio and the dynamic modulus ratio. The purpose of introducing backbone curves is to obtain the shear stiffness G_0 and the damping ratio D which are dependent of the shear strain amplitude.

The backbone curve is mainly influenced by the mean effective stress, the overconsolidation ratio and the plasticity index. In figure 5.1, these parameters are changed to determine which one has the most influence. As it can be noticed in figure 5.1 (middle) the magnitude of overconslidation ratio does not have a significant impact on the backbone curves. The mean effective stress has a significant effect on the backbone curves see Figure 5.1 (left), it increases by increasing the value of the mean effective stress. The plasticity index has the same effect on the backbone curve as the mean effective stress, it increases by increasing its value, see Figure 5.1 (Right).

The backbone curves of the damping ratio and the small-strain stiffness of the soil could be determined from different laboratory methods such as the Bender element test or the Resonant column test, see Determination of small strain shear modulus (G_0) in Chapter 2. Due to insufficient resource and laboratory data, the backbone curves were obtained from the software Strata and research conducted by Darendeli (2001). Strata performs a one

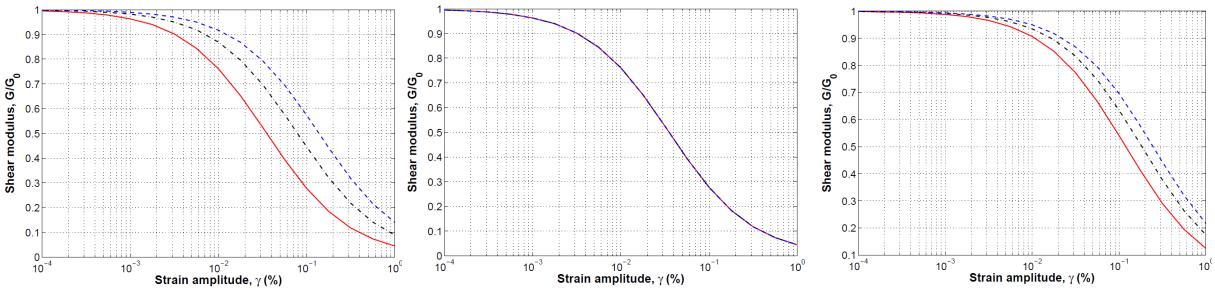

Figure 5.1: Effect of mean effectiv stress (left), Effect of the overconsildation ratio(middle), effect of the plasticity index (right)

Model parameters	1 year	20 years	80 years	120 years
Mean effective stress $[kPa]$	-88.7	-93.6	-95.9	-96.1
Overconsolidation ratio $[-]$	1	1	1	1
Plasticity index $[-]$	35	35	35	35
Excitation frequency $[Hz]$	1	1	1	1
Number of cyles $[N]$	1	1	1	1

Table 5.1: Darendeli and Stokoe model parameters

dimension linear elastic response studies. The stiffness degradation curve and damping ratio used in the backbone curves were obtained from the research mentioned above. The backbone curves for 1, 20, 80 and 120 years were designed under the following assumptions:

The over consolidation ratio is assumed to be 1 since it is supposed that after the construction of the embankment, the excitation frequency for a static case is 1 Hz, the mean effective stress varies depending on the consolidation time and one cycle is considered.

In Figure 5.2, the shear modulus ratio and the damping ratio are presented. Strata has some limitations as the shear modulus ratio and the damping ratio are only based on five different parameters. According to (Benz, 2007), they are actually governed by eleven

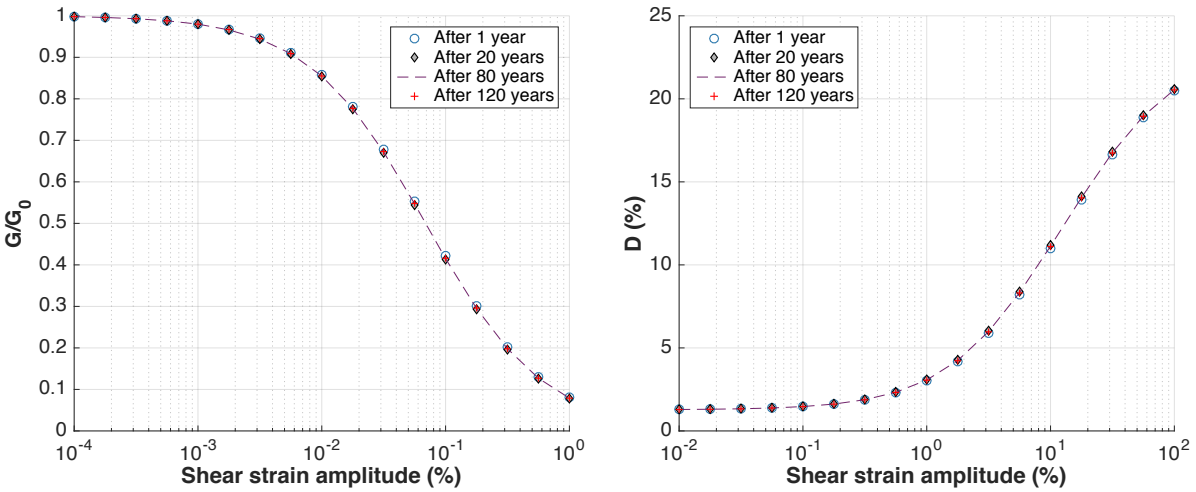

Figure 5.2: Shear modulus ratio (left) and damping ratio (right) according to Strata

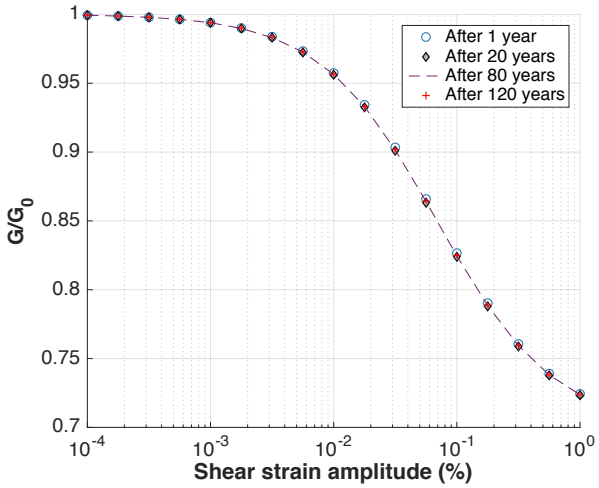

Figure 5.3: Scaled backbone curve for G/G_0

parameters which are the strain amplitude, confining pressure, void ratio, diagenesis, plasticity index, strain rate, effective material stress, degree of saturation, overconsolidation ratio and dilatancy. Strata utilizes mean effective stress, plasticity index, overconsolidation ratio, excitation frequency and the number of cycles.

The backbones curves obtain from Strata represents the original backbones curves generated in lab condition, where a pure shear strain is applied to the soil. While in the real world, the strain applied to the soil is more complex. Considering that the soil's shear modulus can have a maximum decrease of 30 % therefore the backbones curve are scaled, see Figure 5.3.

5.2 Strain

The time dependent strain data was imported from the long term settlement prediction in PLAXIS 2D. In Figure 5.4, the comparison of strain data against depth is shown for 5 different time: 30 days, 150 days, 1, 20 and 120 years after starting the embankment construction. It can be noticed in the figure that the percentage increase in the strain magnitude between 30 - 150 days is larger than 80 - 120 years. This is due to the fact that secondary consolidation occurs over time and the settlement has reached a relatively steady condition.

5.3 Small strain shear modulus

The small strain shear modulus (G_0) can be determined based on the shear wave velocities and the density of the soil, according to Equation 2.4. The density of the soil is assumed to increase linearly with depth, as shown in Equation 5.1:

$$\rho = 1500 - 2.8z \ (z < 0) \tag{5.1}$$

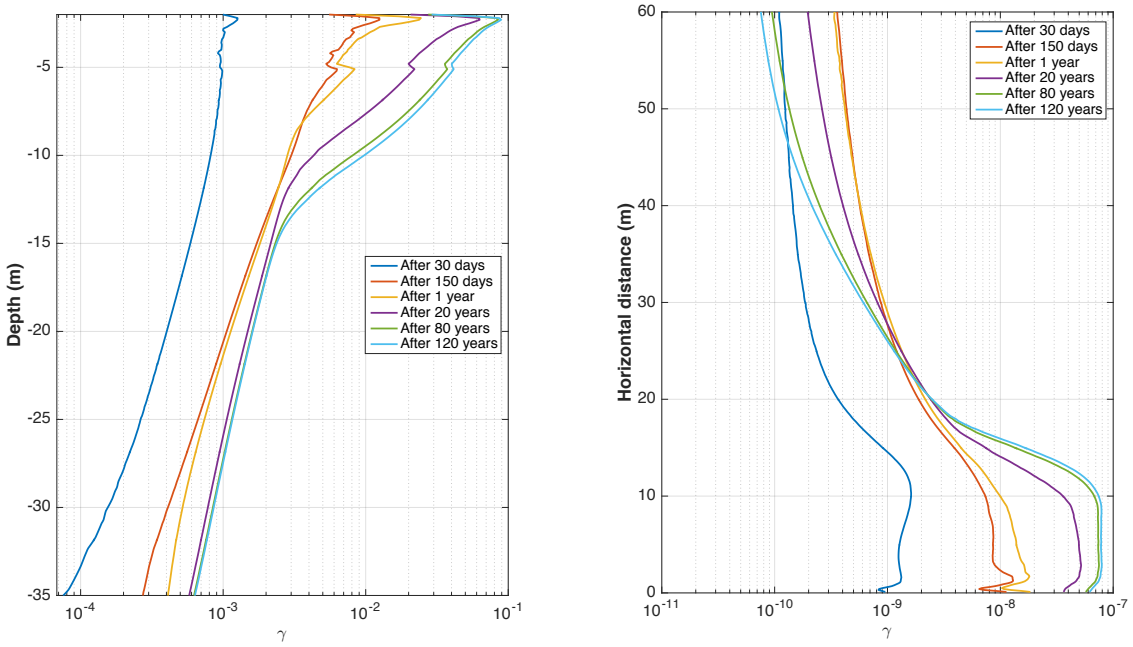

Figure 5.4: Strain distribution from PLAXIS 2D, in the vertical (left) and horizontal (right) direction. The vertical cross-line for the left picture is taken at 0.7 m away from the symmetric center of geometry, the horizontal cross-line for the right picture is at 1 m below the dry crust

The shear wave velocities was obtained from measurements made by (Wood & Dijkstra, 2015) on six different sites in the region of Gothenburg for Swedish clays. This data is presented in Figure 5.5. A polynomial equation is found to best describe the shear wave velocities with respect to the depth z:

$$V_s(z) = p_1 z^7 + p_2 z^6 + p_3 z^5 + p_4 z^4 + p_5 z^3 + p_6 z^2 + p_7 z + p_8 \tag{5.2}$$

The parameters of Equation 5.2 can be found in Appendix C.1 As mentioned previously, the data in Figure 5.5 is for six different sites which in this report was assumed to belong to a specific site. Combining Equation 2.4, 5.1 and 5.2, the small strain shear modulus as a function of depth can be determined, see Figure 5.6.

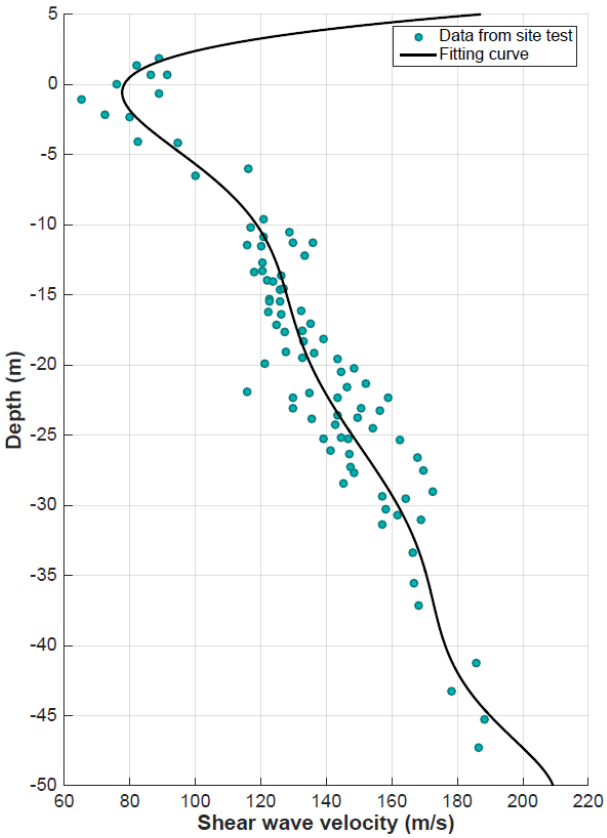

Figure 5.5: Shear waves velocity from different field measurements sites in Gothenburg

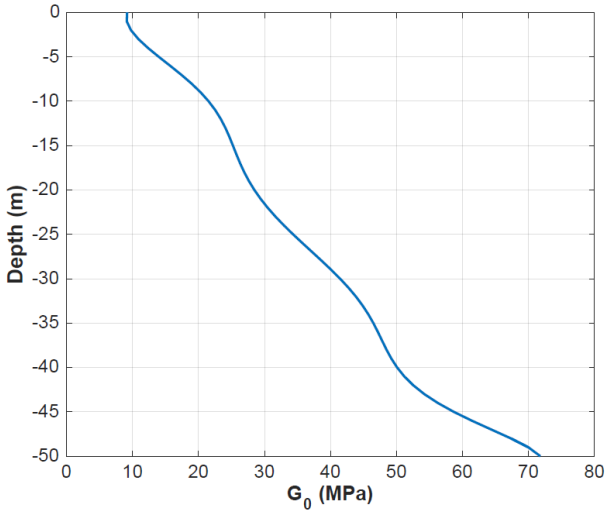

Figure 5.6: Small strain shear modulus depending of the depth

5.4 Combining models

To combine the two models, the dynamic study model in COMSOL Multiphysics has to take into account that the bulk and shear modulus of soil change with vertical and horizontal distances. And so it is for the loss factor of soil. To do this, one can import the

strain data from PLAXIS 2D into COMSOL Multiphysics as an 'interpolation' function of Z (depth) and Y (horizontal distance), and then create functions in COMSOL Multiphysics for the backbone curves, for G_0 which changes with depth, etc. In the end the loss factor and the shear modulus of soil can be achieved through combining these functions.

5.4.1 Function for the backbone curves

The backbone curves for G/G_0 and D (Figure 5.2) are to be implemented in COMSOL Multiphysics. The former is used to calculate the shear modulus of soil, while the latter is used to calculate the loss factor.

To implement the backbone curves in COMSOL Multiphysics, a curve fitting function is generated to match the backbone data from Strata. This is done with the Matlab curve fitting tool. Equation 5.3 and 5.4 are the functions for G/G_0, and for D.

$$f_{g/g0}(x) = 0.7 + 0.3 \times (a_1 sin(b_1 x + c_1) + a_2 sin(b_2 x + c_2) + a_3 sin(b_3 x + c_3)) \tag{5.3}$$

$$f_D(x) = (a_4 sin(b_4 x + c_4) + a_5 sin(b_5 x + c_5) + a_6 sin(b_6 x + c_6)) \tag{5.4}$$

Here $x = log_{10}(100 \cdot \gamma)$. The multiplier 100 accounts for the strain in percentage in the backbone curve. The parameters of this fitting function can be found in Appendix C.3. Figure 5.7 shows that the fitting curve extends the upper range of the variable γ to a maximum of 10 %, which would cover the maximum strain input data from PLAXIS 2D.

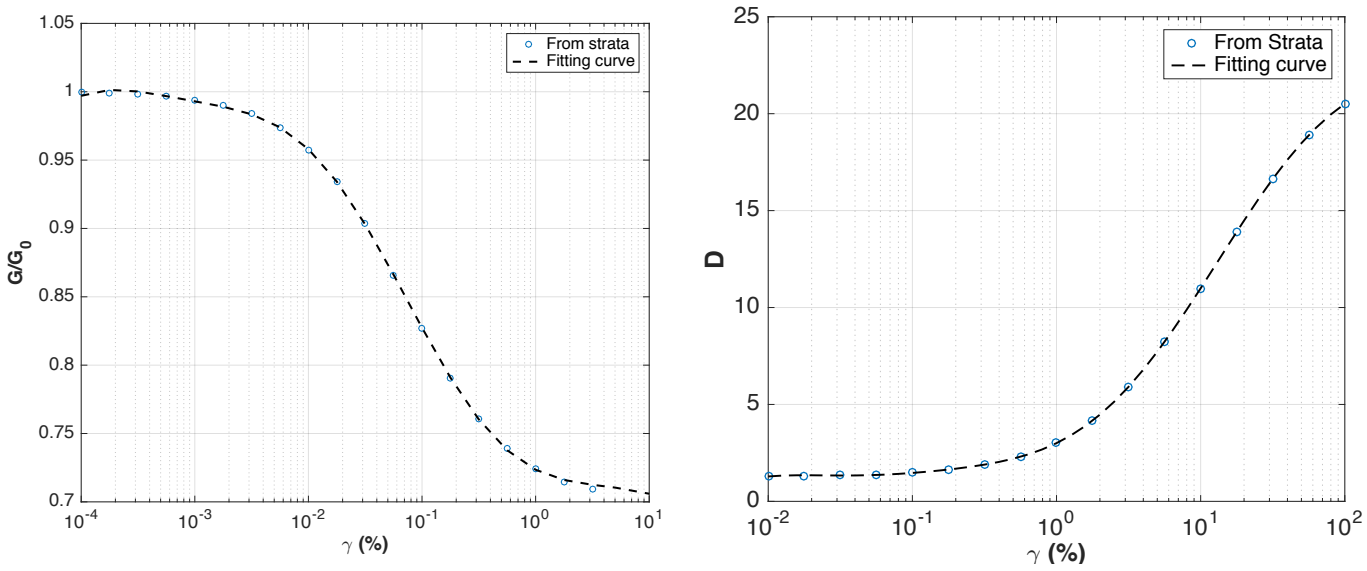

Figure 5.7: Fitting of the backbone curves

5.4.2 Shear modulus

With the shear strain imported in COMSOL Multiphysics, the shear modulus can be calculated through:

$$G = G_0(z) \cdot f_{g/g0}(log_{10}(100 \cdot \gamma)) \tag{5.5}$$

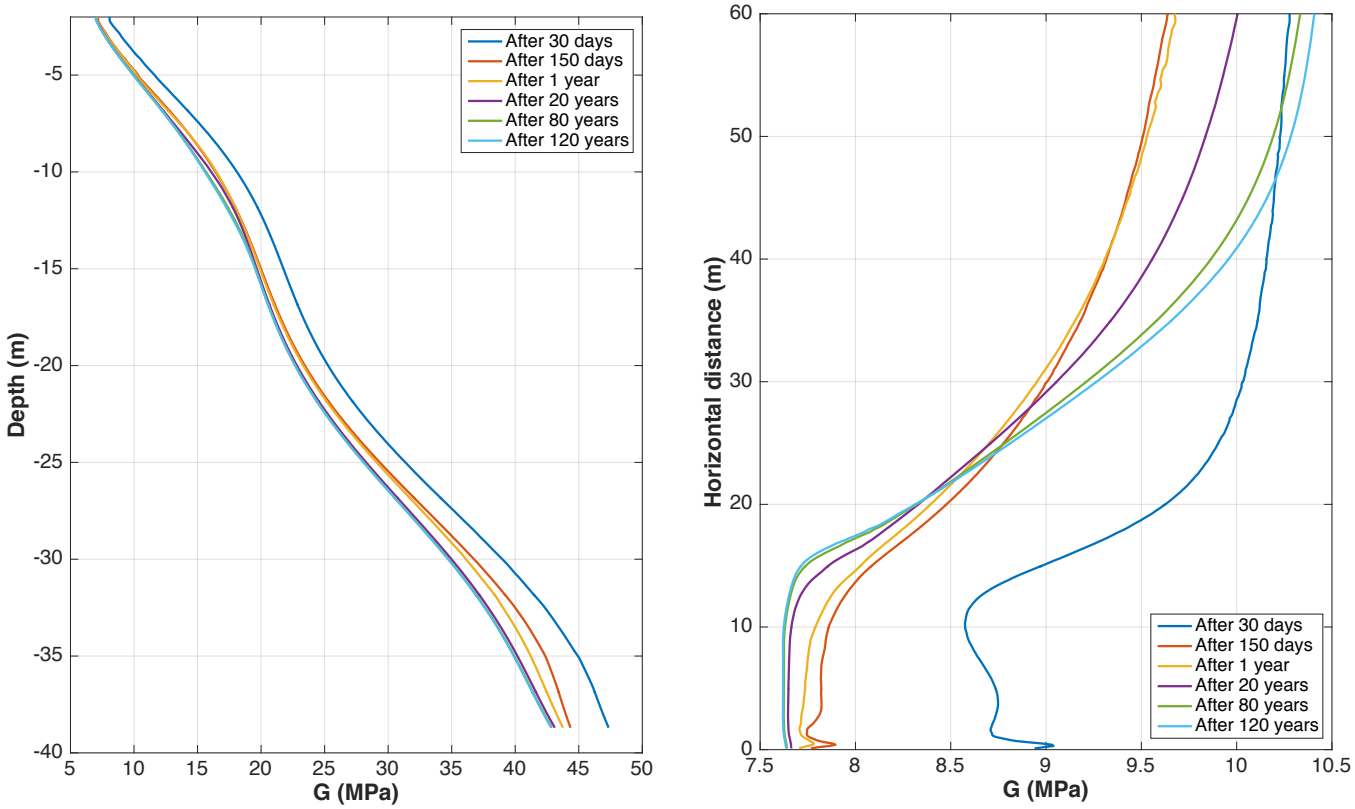

Figure 5.8: Shear modulus distribution in the vertical (left) and horizontal (right) direction, at different time. The vertical cross-line for the left picture is taken at 0.7 m away from the symmetric center of geometry, the horizontal cross-line for the right picture is at 1 m below the dry crust

Figure 5.8 shows the shear modulus calculated from the strain cut-line data in Figure 5.4, to give an idea of how the distribution of shear modulus changes with time. Detailed G distribution can be found in Appendix C.4.

5.4.3 Loss factor

The loss factor is two times the damping ratio given by the degradation curve:

$$\eta = 2 * f_D(log_{10}(100 \cdot \gamma)) \tag{5.6}$$

The loss factor distribution for different times are presented in Appendix C.5

5.4.4 Geometry and material properties

A dynamic model of the railway foundation is built in COMSOL Multiphysics, the geometry of which is shown in Figure 5.9. The model consists of 5 components: the track slab, the concrete base, the embankment, dry crust, and the soft clay. The ground is modelled

with a 40 m radius half-sphere, which is divided into 2 layers by an x-y plane at z = -2 m, to represent the dry crust and soft clay. The embankment is created on a workplane along x-z direction and then extruded for 14 m along x direction.

The track slab is subject to a vertical impact force (1 N), which is positioned 0.6 m away from the edge. 6 positions (see Figure 5.9 left) are chosen to study their transfer functions.

A symmetric boundary constraint is applied on the cross section, and a low-reflecting boundary condition is applied on the outer surface of the half-sphere. The rest of the boundaries are free.

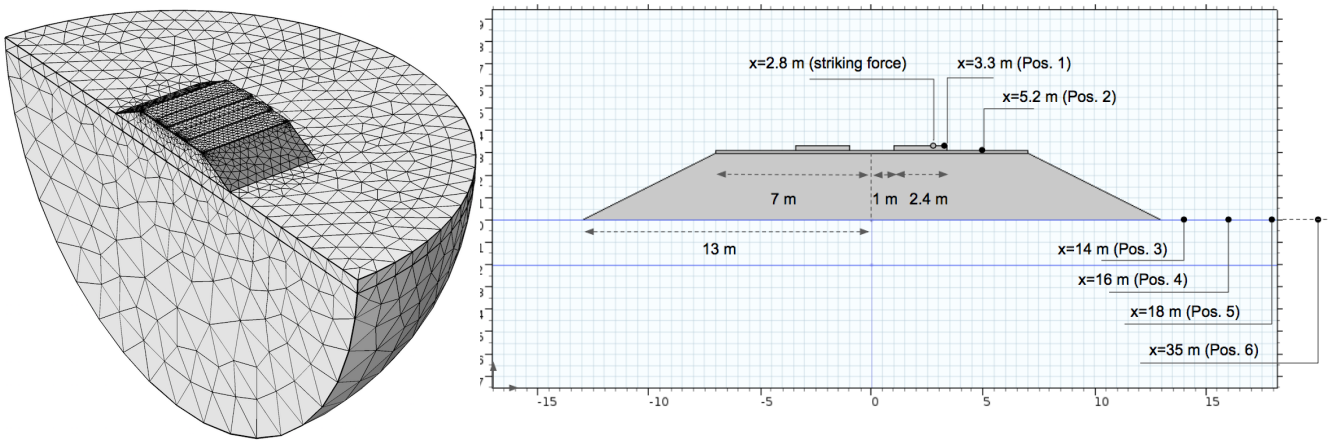

Figure 5.9: Acceleration level at position 1 and 2

The material properties are listed in the following table. h refers to the thickness of the components.

Material	ρ (kg/m^3)	E (MPa)	ν $(-)$	η	h (m)
Track slab	2450	$35 * 10^3$	0.3	0.04	0.21
Concrete base	2300	$33 * 10^3$	0.167	0.04	0.14
Embankment	2200	25	0.25	0.06	3
Dry crust	1800	7	0.30	0.06	2
Soft clay	1500-z*2.8	from PLAXIS 2D	0.4976	from PLAXIS 2D	infinity

Table 5.2: Material parameters for the railway foundation

5.4.5 Mesh

The mesh is generated by COMSOL Multiphysics 'Physics-controlled mesh', with a 'fine' mesh quality. The mesh properties of different components are listed in Table 5.3. The mesh size of track slab and concrete base, which is similar to the validation model, assures that the results are valid up to approximately 280 Hz.

The shear wave speed in the dry crust is calculated to be 38.6 m/s. Therefore the current mesh size in the dry crust can only capture frequencies up to 2.01 Hz. This is much lower than the frequency range in the presented results. This can be a limitation for the results.

Material	Avg mesh size (m)	Number of elements	Avg mesh quality
Track slab	0.744	1145	0.40
Concrete base	0.751	2919	0.24
Embankment	1.257	6497	0.69
Dry crust	3.210	2566	0.66
Soft clay	5.716	6160	0.73

Table 5.3: Mesh properties

5.5 Results of the dynamic model

The dynamic response of the foundation and ground of 4 different points in time (150 days, 1 year, 20 years, and 120 years after the starting day of the embankment construction) are compared with their acceleration levels in vertical direction, with a reference value of $10^{-6} m/s^2$. The embankment construction was complete at 150 days.

5.5.1 Transfer inertance on the track slab and concrete base

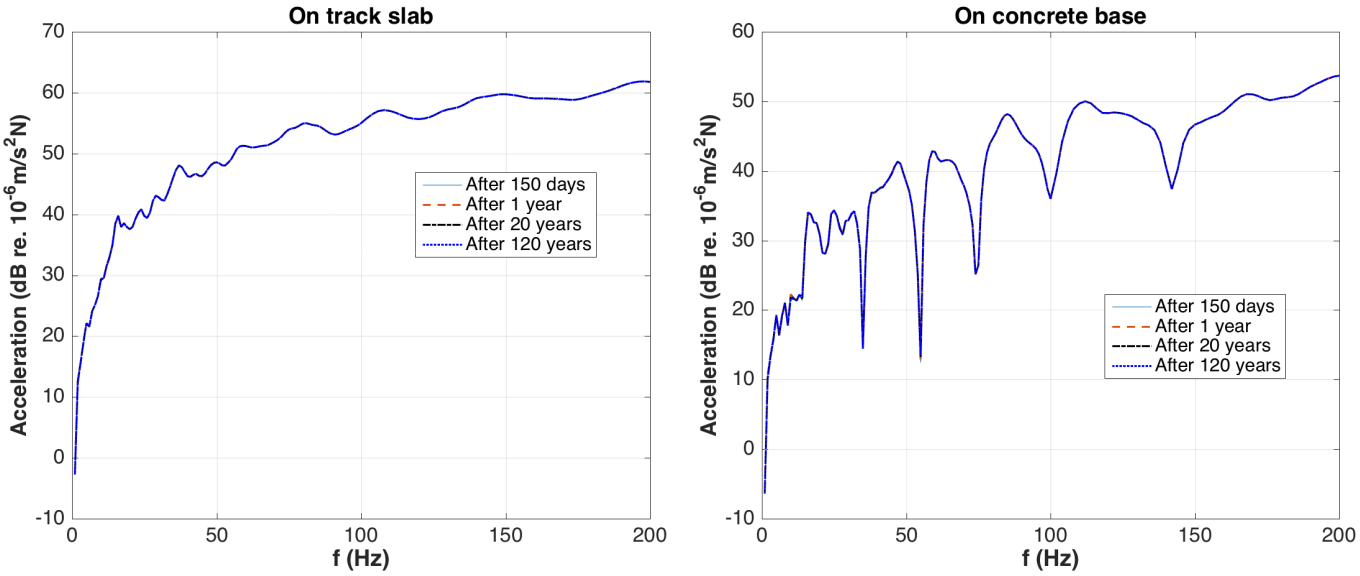

Figure 5.10: Acceleration level at position 1 and 2

Figure 5.10 shows the response on the track slab and on the concrete base. No major difference can be seen among the 4 different points in time. Therefore the level difference of the three later cases compared to the results of after 150 days is plotted in Figure 5.11 to provide more information.

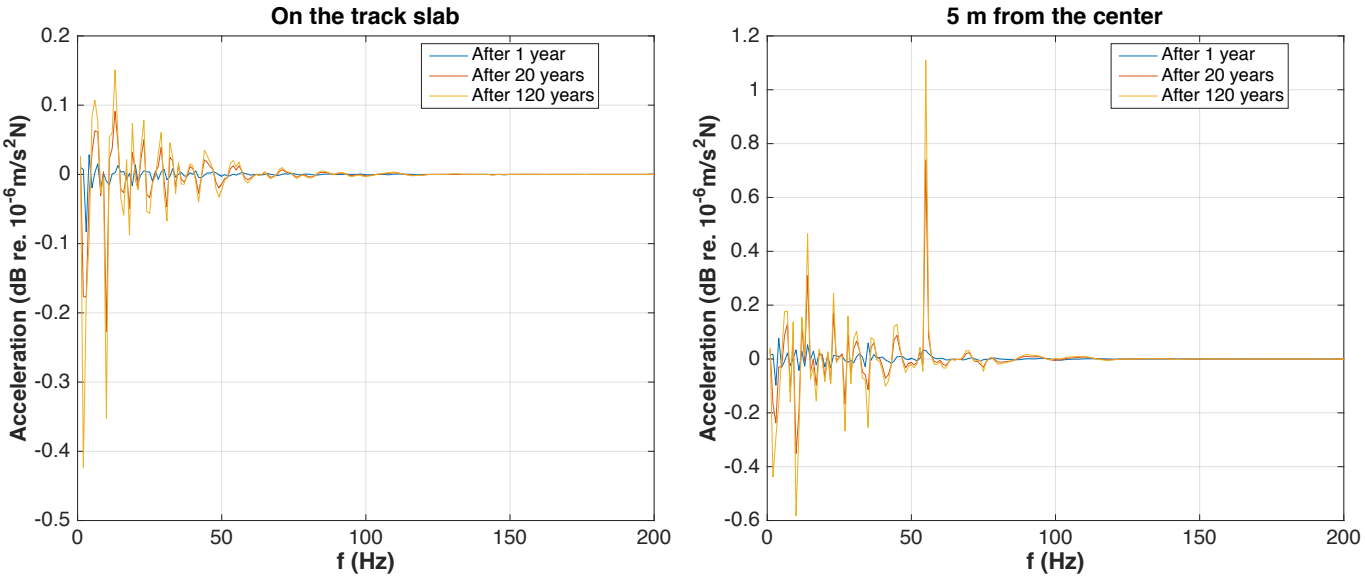

Figure 5.11: Acceleration level at position 1 and 2

Looking at the level difference among the 4 cases, on the track slab, the maximum changes in the acceleration amplitude between 'After 120 years' and 'After 150 days' is around 1.5 %, which happens at 13 Hz. On the concrete base, a maximum of 12 % changes between 'After 120 years' and 'After 150 days' can be seen at 55 Hz. It is also worth notice that the increase or decrease of the acceleration amplitude tends to happen at the same frequencies. But in general the influence on the dynamic response of the track slab due to soil consolidation over years is very small.

5.5.2 Transfer inertance on the surface of ground

The inertance of 4 positions, 1 m, 3 m, 5 m and 12 m away from the embankment (which corresponds to 14, 16, 18 and 35 m away from the center of geometry) are shown in Figure 5.12 and 5.13.

The difference in the magnitude of inertance due to soil consolidation with time is more visible on the ground surface than on the track slab. In general, the dynamic response of low frequencies (below 50 Hz) are less affected by the soil consolidation with respect to time. Most visible changes happen at above 50 Hz. Moreover, the changes in acceleration levels between different times are more prominent as the distance to the embankment increases.

As time increases, the magnitude of inertance at higher frequencies has a general trend of decreasing in all 4 plots. Looking at the results of 5 m away from the embankment, a maximum of 10 dB difference decrease in the magnitude of inertance can be observed from after 1 year to after 20 years, while the change between after 150 days and after 1 year is almost trivial. This is related to the reduction of soil's shear modulus with respect to time, which can be seen in Figure 5.8.

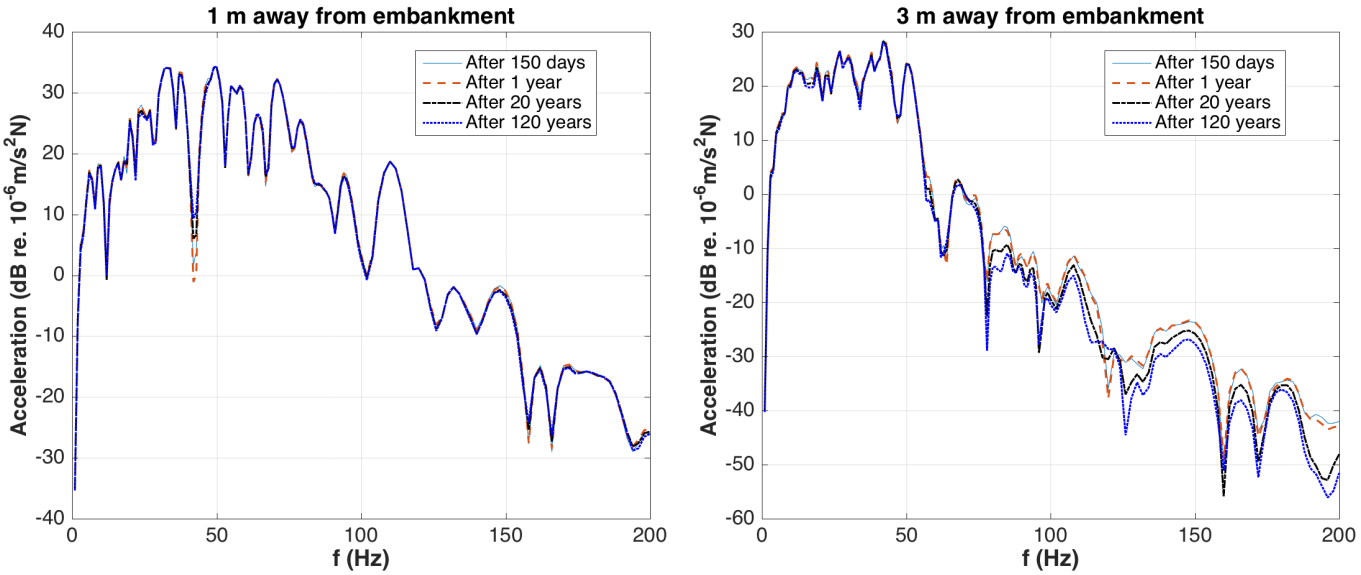

Figure 5.12: Acceleration level at position 3 (1 m away from embankment) and 4 (3 m away)

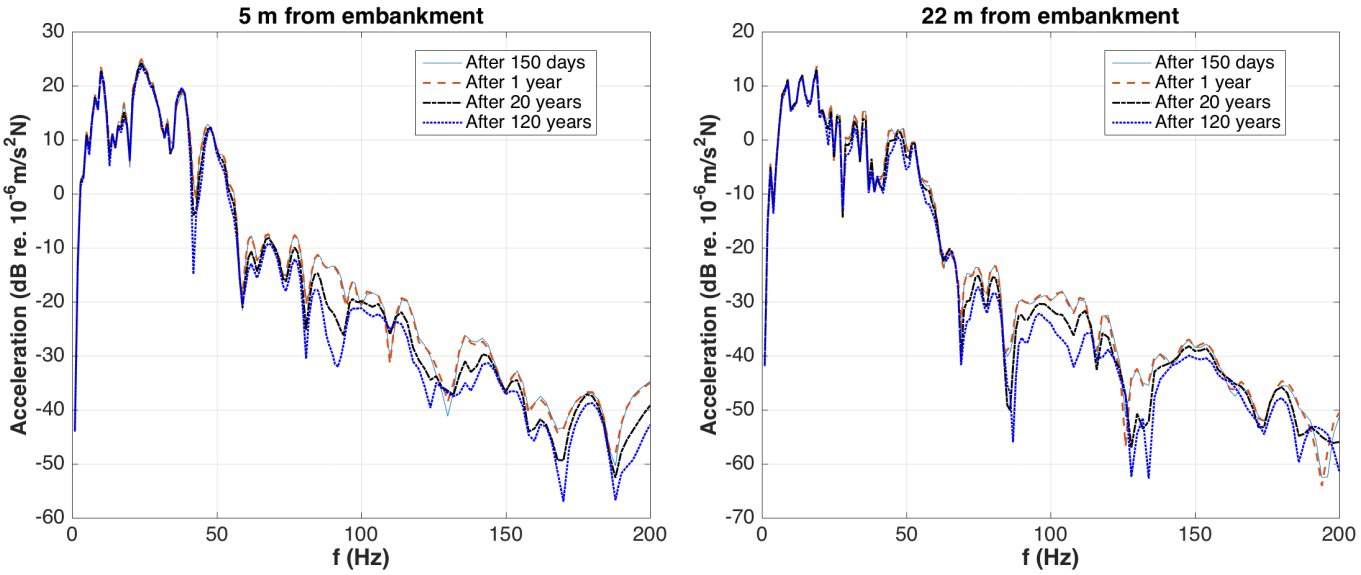

Figure 5.13: Acceleration level at position 5 (5 m away) and 6 (12 m away)

5.5.3 Transfer inertance beneath the embankment

Figure 5.14 shows the transfer inertance of two positions beneath the impact position, at 2 m and 5 m below the ground surface.

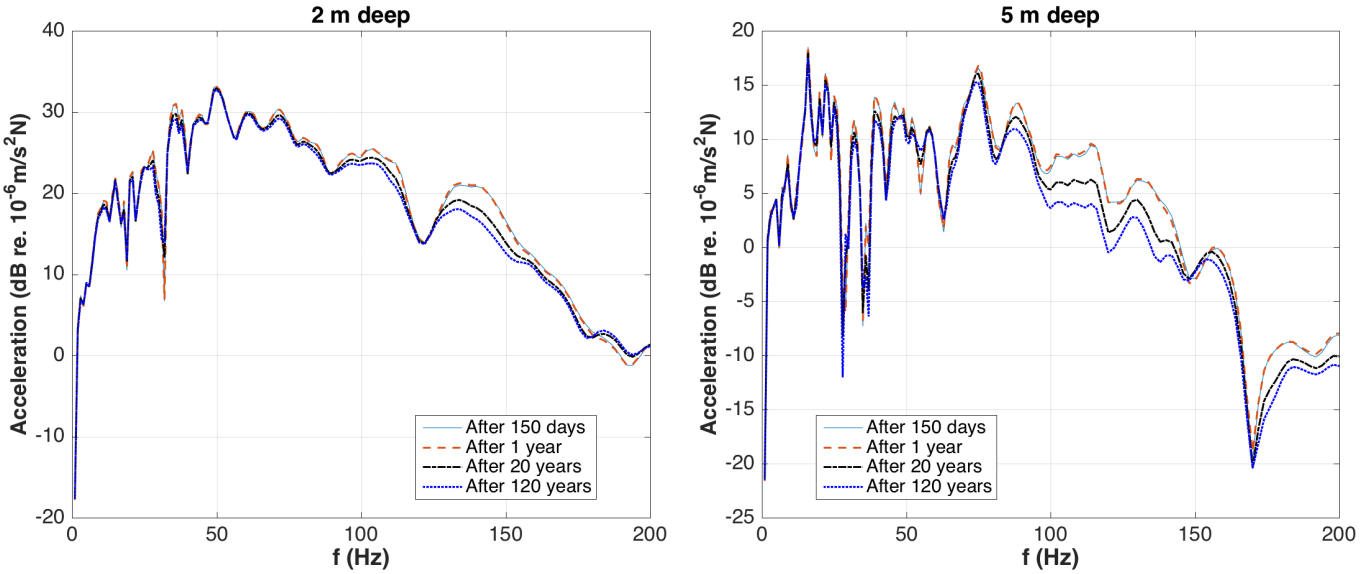

Figure 5.14: Acceleration level at 2 m deep and 5 m deep

Similar trends can be observed compare to the results from the ground surface, in that more visible difference of the acceleration levels between times happens at higher frequencies that lower frequencies, and it increases with the depth of measurement position.

Looking at the results at 2 m depth, for frequencies below 50 Hz, the resonance and anti-resonance peaks for later times (after 20, 120 years) are shallower compared to earlier times (after 150 days, 1 year). This can be explained with the increased loss factor in soil as time increases. Similar observation can be made for the result at 5 m depth, except at the anti-resonance peaks at 26 Hz and 32 Hz, where results from later times are sharper and deeper.

Chapter 6

Discussion

6.1 On the settlement and safety of the embankment

The settlement of the railway foundation after its service life due to solely the embankment weight, without any train load, was predicted to be approximately 500 mm. This is under the assumption that the embankment was constructed in four stages with 30 days between the constructions of the subsequent stage. However, Trafikverkets requirement is 30mm. This settlement should also account for 10 trains per hour. If the model used was to account for moving load, the settlement would be higher.

Even though the settlement predicted is considerably greater than the allowed one, it was expected as no ground improvement was considered in this thesis. Ground improvement will reduce the settlement, especially in this case as the soil if soft clay. Further investigations are required to determine the optimal ground improvement method.

6.2 On the dynamic response of embankment and ground

In this model, the shear modulus of the dry crust layer is smaller than both the embankment above it and the clay beneath it; the change in shear modulus between the embankment and the dry crust is quite enormous. This impedance mismatch causes vibration isolations at low frequencies - the dry crust acts like a sponge layer, and reflections at higher frequencies: vibration levels in the ground generally decrease at above 50 Hz.

What follows is that the soft soil below the dry crust could have a secondary influence on the input impedance at the top of the concrete slab, since there is less energy transmitted from the embankment to the soil. This explains why there are not much differences on the dynamic response of the slab at different times. Moreover, the reinforced concrete slabs and concrete base have very high stiffness, compare to which the changes in the stiffness of the soft soil throughout time is almost negligible.

As time increases, the shear modulus distribution in the soil changes in an interesting way: it decreases at close to the embankment, and increases at far away from the embankment, creating a larger gradient along the ground surface. This increasing shear modulus gradi-

ent along time could account for the decrease in vibration levels, which is quite prominent at higher frequencies (see Figure 5.12 - 5.14). Also, the loss factor increases along time, which also adds to this effect.

6.3 Assumptions and uncertainties

Assumptions were required as there were no soil samples carried out in the investigated area. The soil properties were assumed to be exactly the same as for a current research project in the outskirts of Gothenburg. All parameters except the OCR were assumed to be constant with depth, see table 3.2. The OCR is a sensitive parameter, a higher OCR will result in considerably lower settlements and vice versa, see figure 3.7.

The PLAXIS 2D and the COMSOL Multiphysics model were combined by means of the degradation curve of the soil. This curve obtained from STRATA was modified since the laboratory experiment assumed pure shear strain.

Furthermore, inaccuracies arose when exporting and importing data to different softwares. Since the two softwares use different meshes, when the strain data from PLAXIS is imported, COMSOL uses a linear interpolation method to map the strain data onto its own mesh. Also, assumptions and simplifications have to be made when combining the two models. For instance, the combined model does not take into account the geometry change due to the settlement of the embankment; it also does not consider the ground water level or pore pressure, since these information are assumed to be included in the strain data. These inaccuracies are expected to be insignificant and will therefore not result in a high variation of the final result. For future research, it is recommended to use the same softwares to be able to compare the results. It was decided to use different softwares as PLAXIS 2D is recommended to study the behavior of soil whereas COMSOL Multiphysics is recommended for dynamic studies. Even though it is possible to carry out the studies of this thesis in one software, it was decided to combine them to obtain a more accurate result.

One limitation of the combined model lies in the mesh size of the soil and dry crust in the FE model. The shear wave velocity is 38.7 m/s in the dry crust, and 80 - 180 m/s in the soft clay, varying over depth. The Young's modulus of the dry crust presented in Table 3.1, was chosen as a low bound value due to uncertainty of the dry crust stiffness. The shear wave velocity is dependent of the Young's modulus, which results in a lower shear wave velocity. This results in a relatively small wavelength that requires a even smaller mesh size to capture this frequency. For instance, the wavelength for 100 Hz in the dry crust is 0.3 m, which requires the mesh size to be 1/3 of it (considering the mesh's discretization order is quadratic): 0.1 m. Due to the large volume of the ground to be meshed, and limitation of computation power, the chosen mesh size is of the best precision than can be calculated. The assumption is that the calculation at higher frequencies still provides a valid comparison study between different times, albeit the insufficient mesh size.

Chapter 7

Conclusions & Recommendations

7.1 Conclusions

The settlement prediction due to solely the weight of the railway embankment is approximately 500 mm, at the end of its service life. This is considerably larger than the requirement of Trafikverket of 30 mm. However, it is within expectation, since no ground improvement was considered.

The combined dynamic model shows that, due to small changes in the soil's shear modulus during the service life of the embankment, and that the dry crust were extremely soft, there will be no major differences on the dynamic response of the track slab. A stiffer dry crust layer is expected to give larger influence. Also, a decrease in vibration levels at ground surface can be observed as time increases. However, the combined dynamic model suffers from uncertainties such as insufficient mesh size, the boundary condition at the edge could be better characterised, etc., which prevent the authors from drawing solid conclusions from the results produced by this model.

The work shows that geotechnical and ground vibration studies can be combined by taking into account the changed moduli and loss factor of soil during the slow process in the dynamic analysis.

7.2 Recommendations

For further research, the following recommendations are proposed:

- Perform appropriate laboratory tests to obtain specific soil data such as the resonant column test or the bender element test to obtain the backbone curves.
- Further investigations to study the stability of the embankment under dynamic loading.
- The settlement predicted by the PLAXIS 2D model was larger than the requirement of Trafikverket, further investigations are required to determine the optimal ground improvement method.

- Further investigations to study the behavior of pore water pressure and residual stress accumulation on different loading frequencies and the number of cycles.
- The combined model is, at the moment, a one-way collaboration: the effect of the dynamic loading process to the soil was not considered. This can be considered in future works.
- A larger and finer FE model should be used to provide more accurate results in the future, also the effect of the boundary condition representing an infinite ground should be better studied.
- A lot of simplifications have been made when building the combined model, e.g. the geometry deformation of the ground and embankment due to settlement was not considered. Also, the combined model applies a linear-elastic physics, which ignores other properties of soil such as ground water level, pore pressure, etc. This leaves space for future improvement.
- It is of future interest to study the dynamics of the embankment under a moving load excitation, which resembles a passing-by train.

References

Asslan, M. (2008). Factors Influencing Small-Strain Stiffness of soils and its Determination. In M. Asslan, Factors Influencing Small-Strain Stiffness of soils and its Determination (pp. 41-56). Wimar: Bauhaus-Universität Weimar.

Axelsson, M. (2016). Nya stambanor Höghastighetsjärnväg. BIG seminarium (pp. 1-14). Solna: Trafikverket.

Baidya, D.K., Muralikrishna, G. & Pradhan, P. K. (2006) Investigation of foundation vibrations resting on a layered soil system J. Geotech. Geoenviron. Eng., vol.132, no. 1, pp. 116-123.

Baidya, D. K. and Krishna, G. M. (2001) Investiga- tion of Resonant Frequency and Amplitude of Vibrating Foot- ing Resting on a Layered Soil System, Geotechnical Testing Journal, GTJODJ, Vol. 24, No. 4, pp. 409-417.

Benz, T. (2007) Small-Strain Stiffness of Soils and its Numerical Consequences. Mitteilung 55 edn. Stuttgart: Institut für Geotechnik der Universität Stuttgart.

Bjerrum, L. (1973). Bjerrum, L. (1975) 'Problems of soil mechanics and construction on soft clays and structurally unstable soils-collapsible expansive and others', International Journal of Rock Mechanics and Mining Sciences & Geomechanics Abstracts, 12(2), pp. 111–160.

Brinkgreve, R., Kappert, M., & Bonnier, P. (2007). Hysteretic damping in a small-strain stiffness model. Numerical Models in Geomechanics, pp. 737-742.

Brinkgreve, R., Kumarswamy, S., & Swolfs, W. (2016). Tutorial Manual PLAXIS 2D 2016. Construction of a road embankment. Netherlands: Delft University of Technology & PLAXIS bv, pp. 61-78.

Darendeli, M. B. (2001). Development of a new family of normalized modulus reduction and material damping. Texas: University of Texas at Austin.

Drnevich, V.P., Werden, S., Ashlock, J.C. and Hall, J.R. (2014) 'Applications of the new approach to resonant column testing', Geotechnical Testing Journal, 38(1), pp. 23-39

Ebrahimian, B. (2013). Numerical Modelling of the Seismic Behaviour of Gravity-Type

Quay Walls. i S. D'Amico, Engineering Seismology, Geotechnical and Structural Earthquake Engineering (Chapter 11). Tehran: University of Tehran.

Fang, M., & Cerdas, S. F. (2015). Theoretical analysis on ground vibration attenuation using sub-track asphalt layer in high-speed rails. Springerlink, pp. 214-219.

Gazetas, G. (1983) Analysis of machine foundation vibrations: state of the art, Soil Dynamics and Earthquake Engineering, 2, 2-42.

Grau, L. and Laulagnet, B. (2015a) Ground cross-modal impedance as a tool for analyzing ground/plate interaction and ground wave propagation. J, Acoust. Soc. Am, 137(5), May 2015.

Grau, L. (2015b) Approche analytique modale pour la prévision vibratoire de plaques couplées à des sols: Applications ferroviaires, Vibrations [physics.class-ph]. INSA Lyon. Francais.

Griesmer, A. (2014) Size parameters for free tetrahedral meshing in COMSOL Multiphysics. Available from: <https://www.comsol.se/blogs/size-parameters-free-tetrahedral-meshing-comsol-multiphysics/>.

Gucunski, N. and Peek, R. (1993) Vertical vibrations of circular flexible foundations on layered media. Soil Dynamics and Earthquake Engineering (Vol. 12, pp. 183-192).

Gutowski, T.G. and Dym, C.L. (1976) Propagation of ground vibration: a review. J. Sound & Vib. 49(2), p.179-193.

Hansbo, S. (1975) Jordmateriallära (Soil material science). Stockholm: AWE/GEBERS.

Hardin, B. O., & Drnevich, V. P. (1972). Shear modulus and damping in soils. Journal of the Soil Mechanics and Foundations Division 97, 667-692.

Heckl, M., Hauck, G. and Wettschureck, R. (1996) Structure-borne sound and vibration from rail traffic. J. Sound. & Vib. 193(1), p. 175-184.

Kaufman, A.A. and Levshin, A.L. (2005) Acoustic and Elastic Wave Fields in Geophysics III, 1st Edition, Elsevier Science, Amsterdam.

Kaynia, A.M., Madshus, C., Zackrisson, P. (2000) Ground vibration from high-speed trains: prediction and countermeasure. J. Geotech. Geoenviron. Eng., 126(6), p. 531-537.

Kellett, J. (1974). Terzaghi's theory of one dimensional primary consolidation and its application . Australia: Department of minearals and energy.

Karlsson, M., Bergström, A., & Dijkstra, J. (2015). Comparison of the performance of mini-block and piston sampling in high plasticity clay. Gothenburg: Chalmers

Unuversity of Technology.

Kim, T. C., & Novak, M. (1981). Kim, T.C. and Novak, M. (1981) 'Dynamic properties of some cohesive soils of Ontario', Canadian Geotechnical Journal, 18(3), pp. 371–389.

Krylov, V. V. (2001) Noise And Vibration From High-Speed Trains. London: Thomas Telford, Chap 11.5.

Lamb, H. (1904) On the Propagation of Tremors over the Surface of an Elas- tic Solid, Transactions of the Royal Society of London. Series A, Containing Papers of a Mathematical or Physical Character, Vol. 203 (1904), pp. 1-42

Larsson, R. (1986). Consolidation of soft soils. Linköping, Sweden: Swedish Geotechnical Institute Report 29.

Likitlersuang, S., Teachavorasinskun, S., Surarak, C., Oh, E. and Balasubramaniam, A. (2013) 'Small strain stiffness and stiffness degradation curve of Bangkok clays', Soils and Foundations, 53(4), pp. 498–509.

Lombaert, G., Degrande, D., Francois, S. and Thompson, D.J. (2015) Ground-borne vibration due to railway traffic: a review of excitation mechanisms, prediction methods and mitigation measures.

Lysmer, J. (1965) Vertical Motions of Rigid Footings, Ph.D. thesis, University of Michigan, Ann Arbor

Luna, R., & Jadi, H. (2000). Determination of Dynamic Soil Properties using Geophysics Methods. International Conference of the Application of Geophysics and NDT methodologies to Transportation Facilities and Infrastructure (pp. 1-15). St.Louis: Department of Civil Engineering, University of Missouri.

Länsivaara, T. T. (1999). A study of the mechanical behavior of soft clay. NTNU, Geotechnical Engineering. Trondheim: Norwegian University of Science and Technology.

Mohammad M. Toufigh, A. O. (2009). Soil Dynamics and Earthquake Engineering. i A. O. Mohammad M. Toufigh, Engineering, Soil Dynamics and Earthquake (Vol. 29), pp. 356-363.

Okur, D.V. and Ansal, A. (2007) 'Stiffness degradation of natural fine grained soils during cyclic loading', Soil Dynamics and Earthquake Engineering, 27(9), pp. 843–854.

Olsson, E. (2014) A dynamic response study on piling depth with respect to ground vibrations.

Rampello, S., Viggiani, G.M.B. and Amorosi, A. (1997) 'Small-strain stiffness of reconstituted clay compressed along constant triaxial effective stress ratio paths', Géotechnique, 47(3), pp. 475–489.

Richart, F.E. Jr, Hall, J.R. Jr, & Woods, R.D. (1970) Vibrations of soils and foundations, Prentice-Hall, Englewood Cliffs, NJ.

Sadd, M. H. (1990) Wave Motion and Vibration in Continuous Media. Available from: <https://personal.egr.uri.edu/sadd/mce565/Ch12.pdf>.

Sivasithamparam, N., Karstunen, M. and Bonnier, P. (2015) 'Modelling creep behaviour of anisotropic soft soils', Computers and Geotechnics, 69, pp. 46–57.

Suhairy, S. (2000) Prediction of ground vibration from railways, Swedish National Testing and Research Institute (SP), Acoustics, report 2000: 25.

Sällförs, G. (1975). Preconsolidation pressure of high plastic clays. Gothenburg, Sweden: Chalmers University of Technology.

Sällförs, G. (2001). Geotechnics: Soil material science, Soil mechanics, 3 edition. Gothenburg, Sweden: Chalmers University of Technology.

Track structure. Available from: <http://www.railsystem.net/track-structure/>.

Trafikverket (2015). High speed railway. Retrieved from www.trafikverket.se: http://www.trafikverket.se/en/startpage/planning/high-speed-railway/

Uneklint, P., & Bernström, P. (2015). Sverigeförhandlingen och Nya höghastighetsjärnvägar i Sverige. Samhällsekonomiska nyttor (pp. 14-20). Trafikverket.

Vucetic, M., & Dobry, R. (1991). Vucetic, M. and Dobry, R. (1991) 'Effect of soil plasticity on Cyclic response', Journal of Geotechnical Engineering, 117(1), pp. 89–107.

Wood, D. M. (1990). Soil behaviour and critical state soil mechanics. Cambridge, United Kingdom: Cambridge University Press.

Wood, T., & Dijkstra, J. (2015). On the small strain stiffness of some Swedish clays & Its impact on deep excavations. Gothenburg: Chalmers University of Technology.

Yiqun Tang, J. Z. (2013). Dynamic Response and Deformation Characteristic of Saturated Soft Clay under Subway Vehicle loading. In J. Z. Yiqun Tang, Introduction (p. 10). Shanghai: Tongji University.

Larsson, R. (1986). Zhang, Q. & Yiqun, T. (1994). A study on tuneling technology with access to tunnel for shield. Underground space 14(2)

Appendix A

Soil parameters

Site No.	ρ (kg/m^3)	I_p	W_n (%)	W_p (%)	W_L (%)	$\tau(kPa)$	OCR
1	1550-1680	24-52	71-59	31-26	100-70	15-150	1.6-1.3
2	1540-1640	24-52	84-61	41-31	72-49	19-55	1.44-1.33
3	1520-1660	24-52	94-59	43-27	84-59	21-112	1.4-1.33
4	1610-1910	24-52	66-40	35-24	70-39	37-55	1.65-1.27
5	-	24-52	-	-	-	-	-
6	1500-1800	24-52	100-50	-	95-40	5-90	1.5-1.23
7	1470-1560	24-52	100-74	36-29	99-71	11-25	1.4-1.1
8	1490	24-52	90	-	-	28-30	2

Table A.1: Soil parameters for the different sites

Appendix B

Results from the long term settlement prediction (static case)

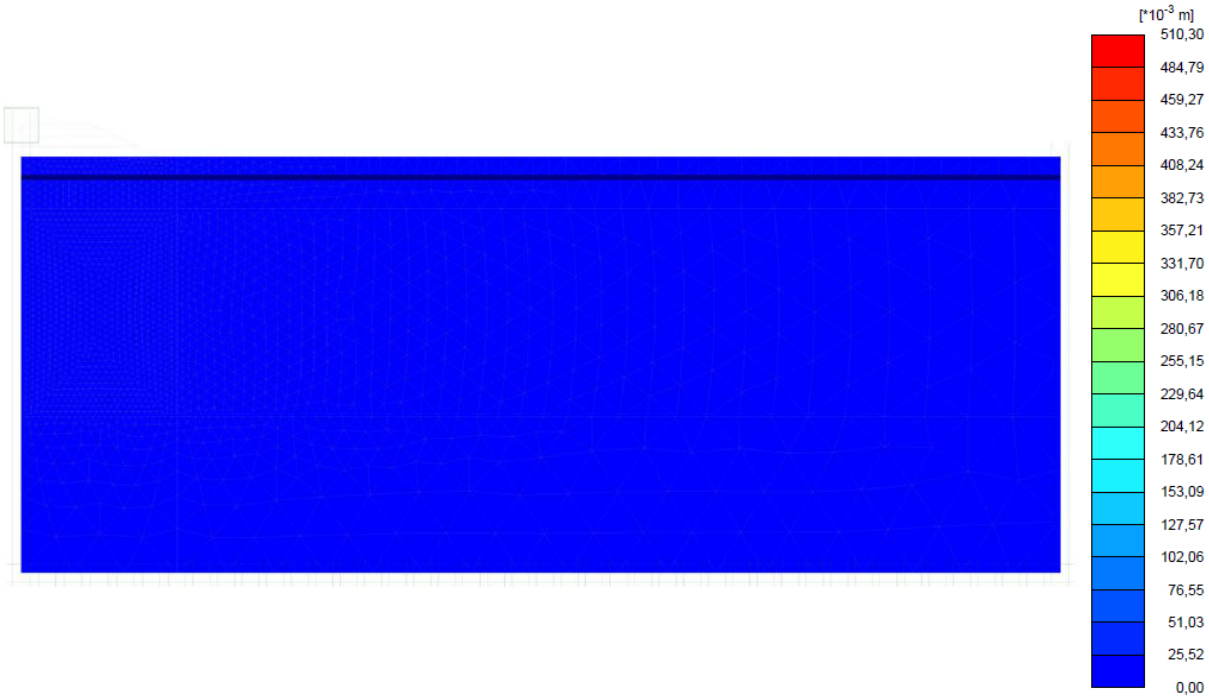

Figure B.1: Maximum vertical displacement under the embankment center line during the initial phase: 0.00 mm

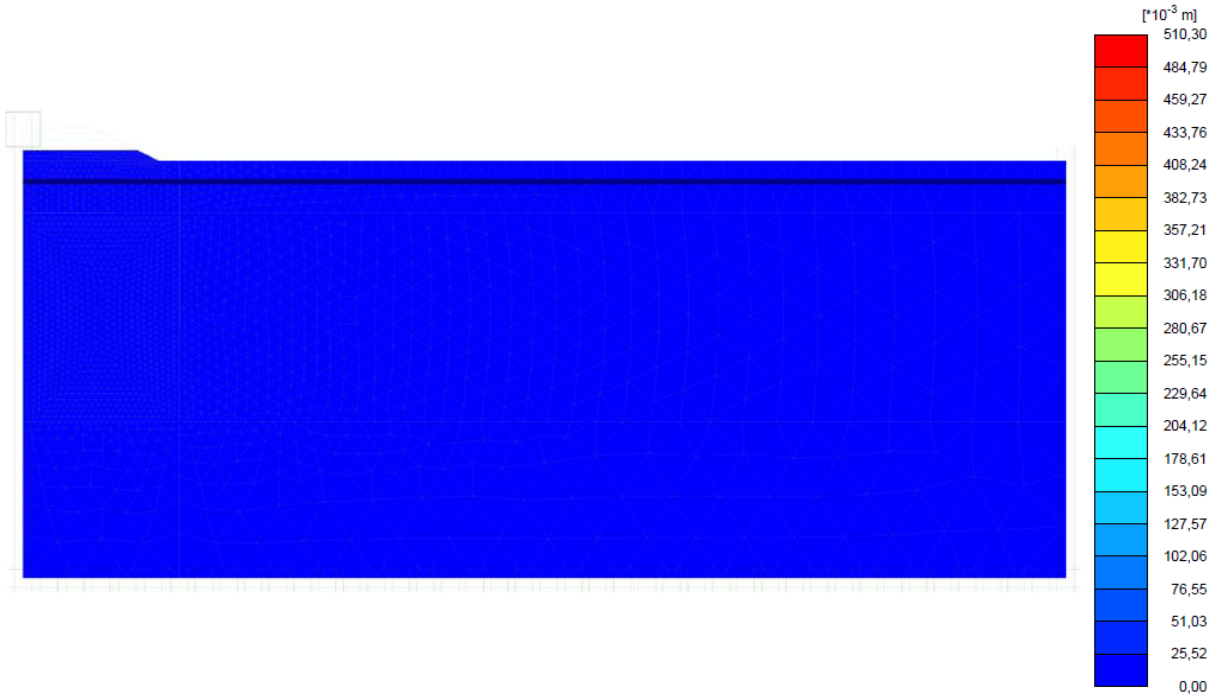

Figure B.2: Maximum vertical displacement under the embankment center line after 30 days: 0.023 mm

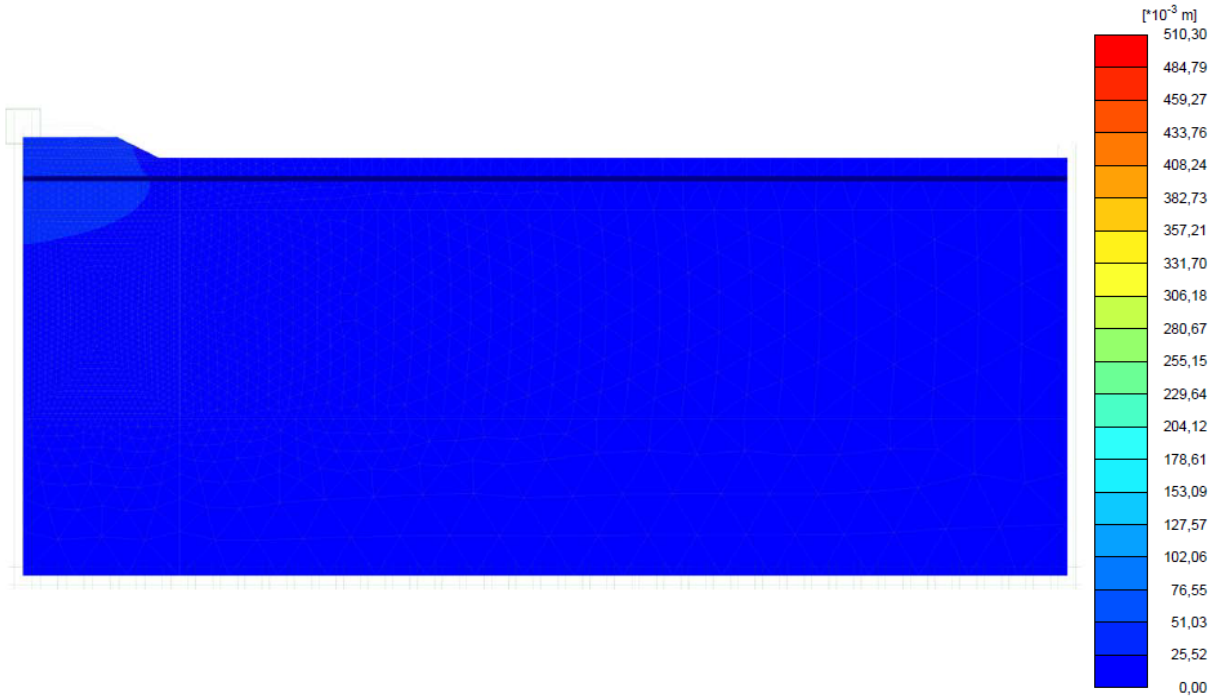

Figure B.3: Maximum vertical displacement under the embankment center line after 60 days: 0.048 mm

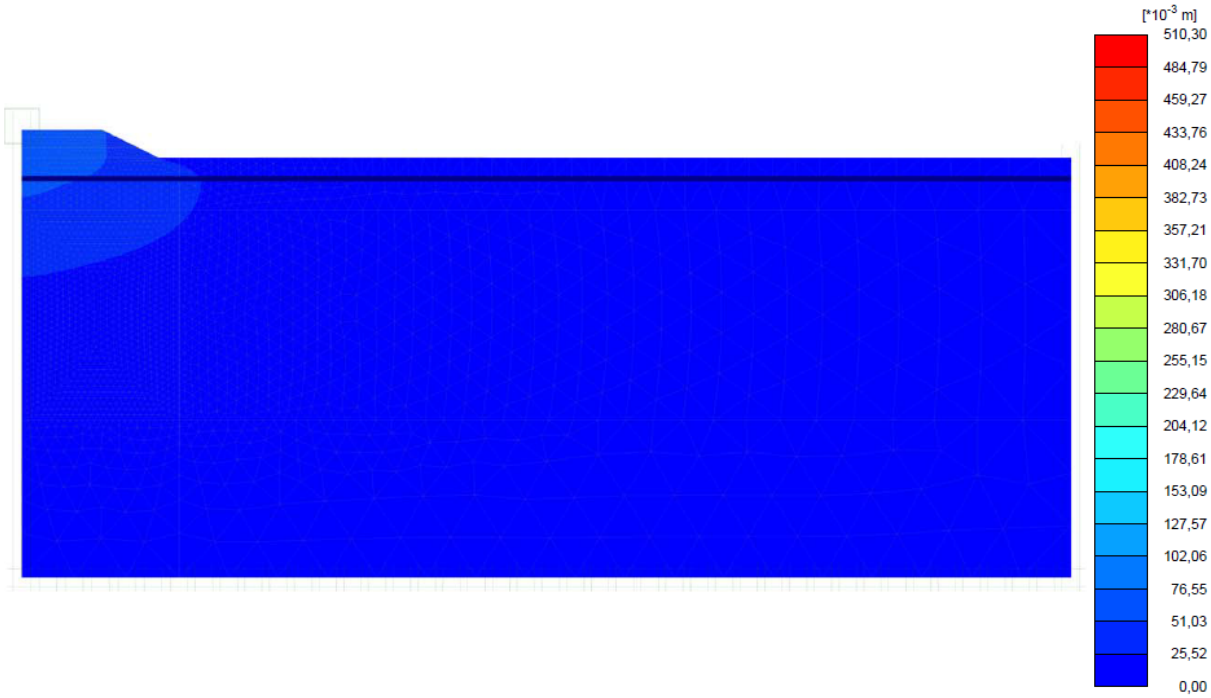

Figure B.4: Maximum vertical displacement under the embankment center line after 90 days: 0.069 mm

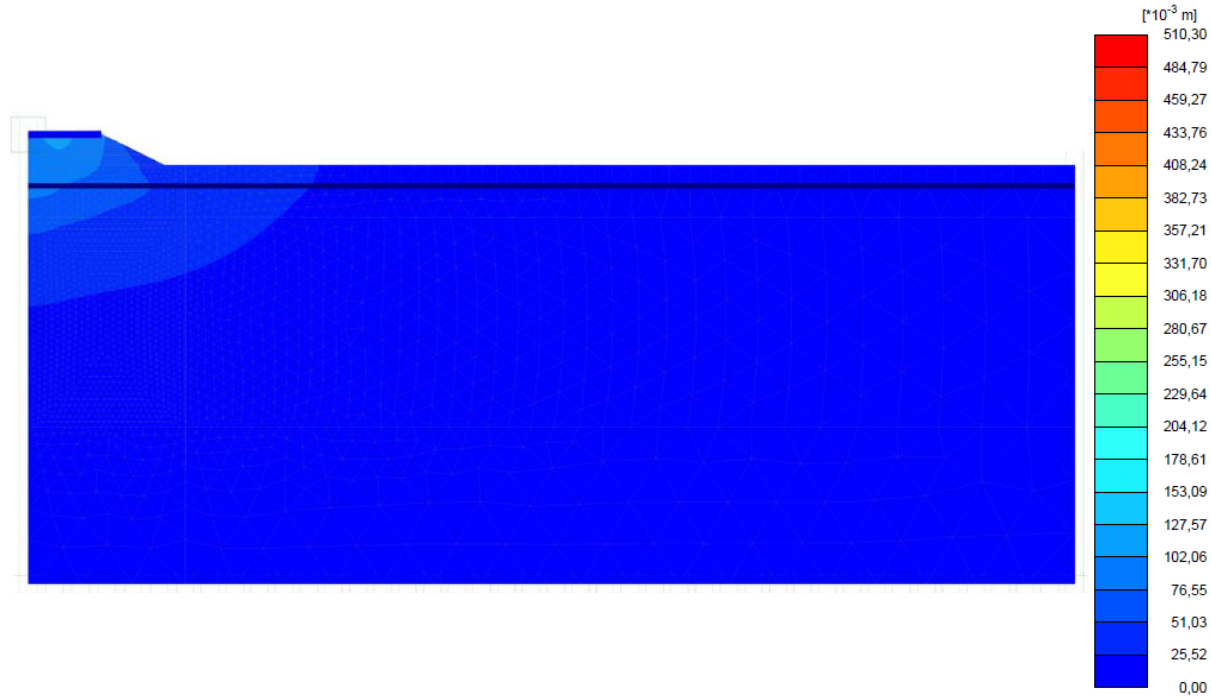

Figure B.5: Maximum vertical displacement under the embankment center line after 150 days: 0.104 mm

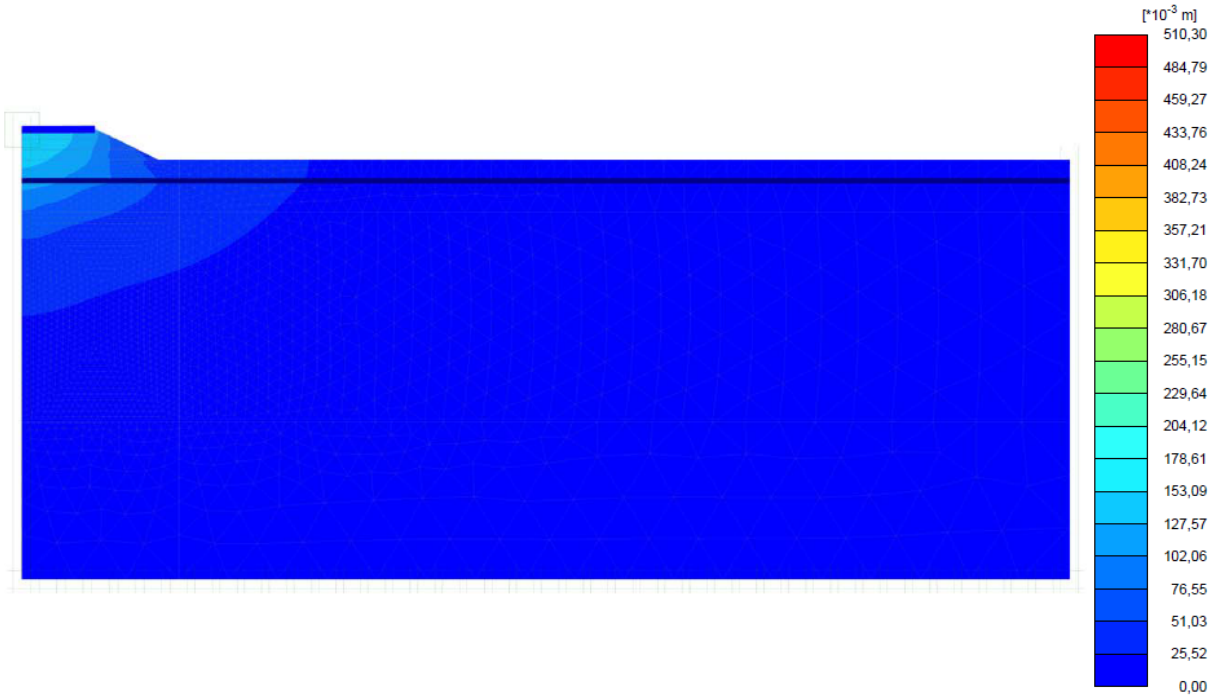

Figure B.6: Maximum vertical displacement under the embankment center line after 1 year: 0.135 mm

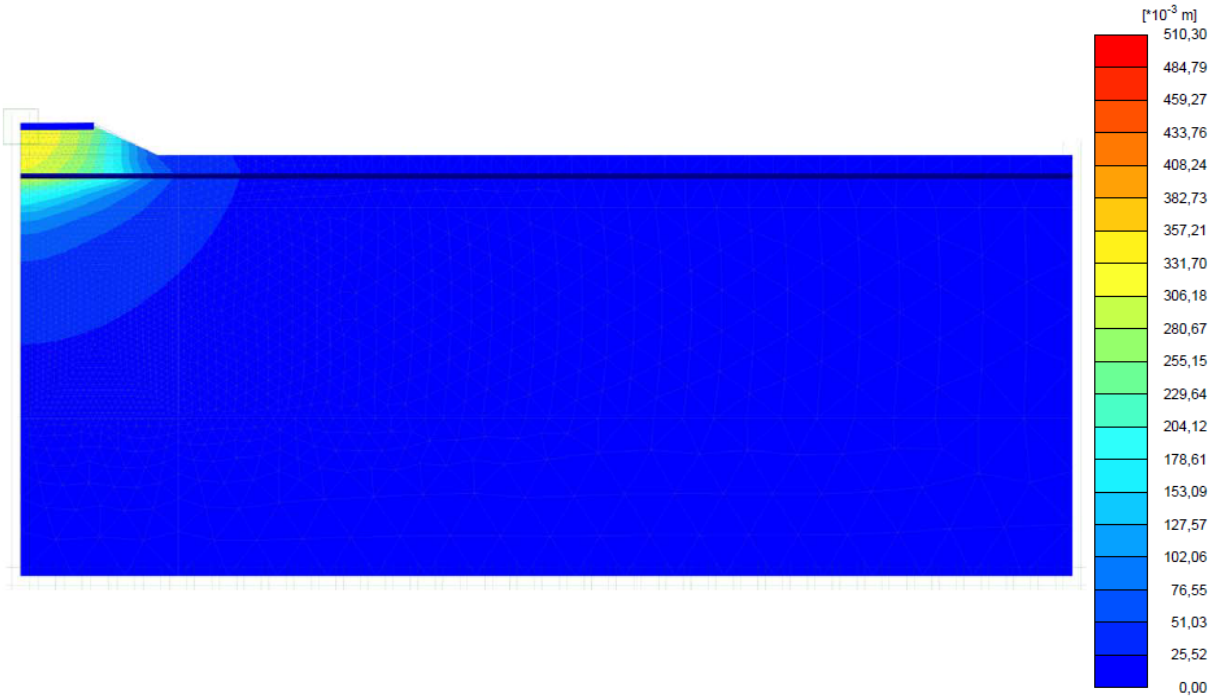

Figure B.7: Maximum vertical displacement under the embankment center line after 20 years: 0.315 mm

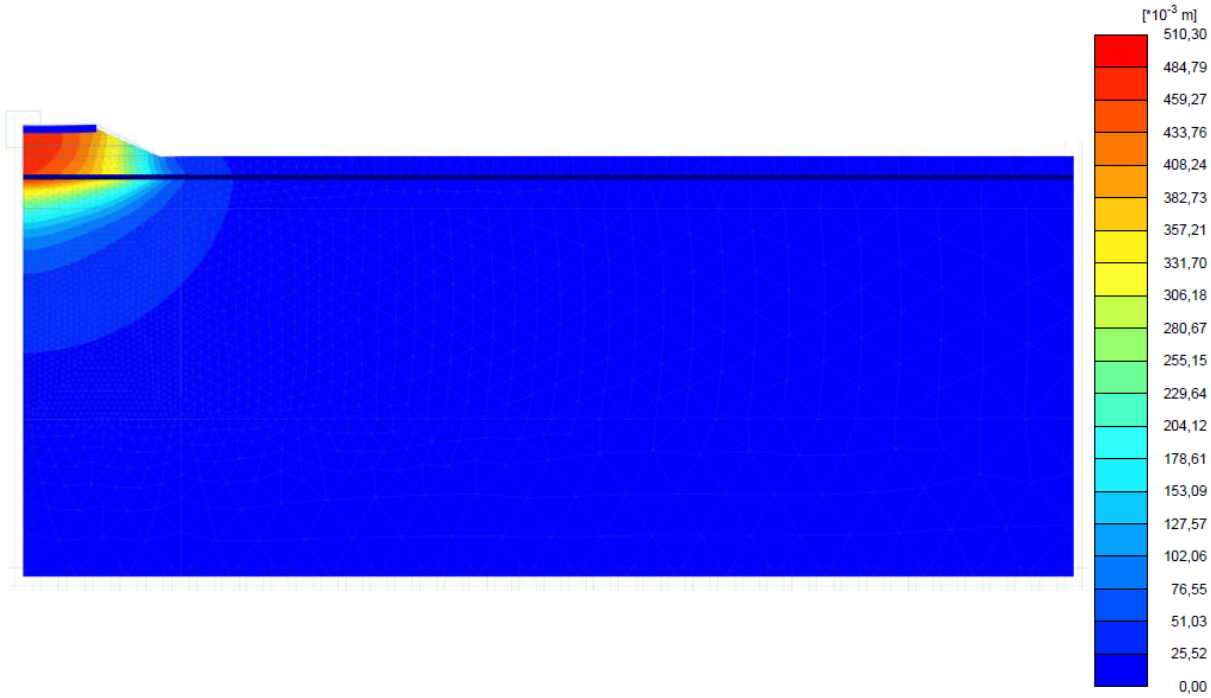

Figure B.8: Maximum vertical displacement under the embankment center line after 80 years: 0.471 mm

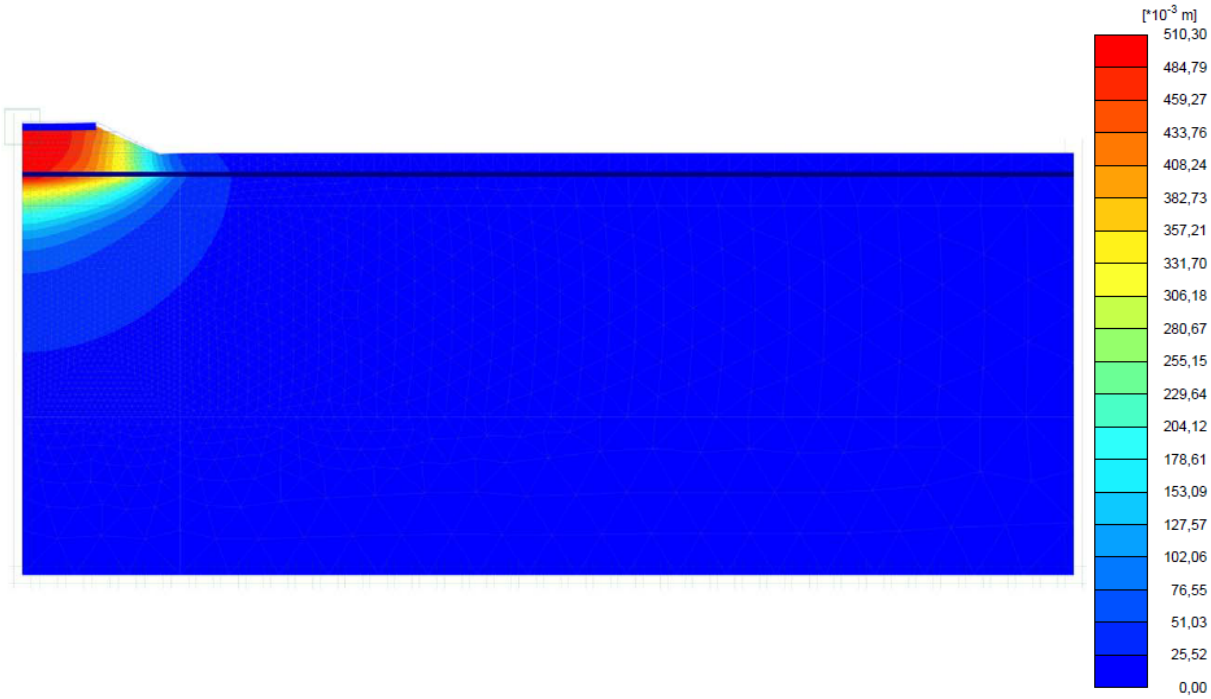

Figure B.9: Maximum vertical displacement under the embankment center line after 120 years: 0.510 mm

Appendix C

Curve fitting data

C.1 Vs - z

p1 = 3.217e-8; p2 = 5.838e-6; p3 = 0.0004163; p4 = 0.01471; p5 = 0.2648; p6 = 2.165; p7 = 2.224; p8 = 78.23;

C.2 Degradation curve - G/G_0

a_1 = 2.56 , b_1 = 0.4728, c_1 = 1.492, a_2 = 2.518, b_2 =0.5531, c_2 = -1.825, a_3 = 0.06252, b_3 = 2.278, c_3 = -0.6266;
Goodness of fit: SSE: 0.0004941 R-square: 0.9998 Adjusted R-square: 0.9997 RMSE: 0.006417

C.3 Degradation curve - D

a_4= 28.4 ;b_4= 0.1695 ;c_4= 0.6011 ;a_5= 4.398 ;b_5= 1.342 ;c_5= 1.188 ;a_6= 0.5281 ;b_6= 2.784 ;c_6= 2.368 ;

Goodness of fit: SSE: 0.005567 R-square: 1 Adjusted R-square: 1 RMSE: 0.02359

C.4 G distribution in the combined model

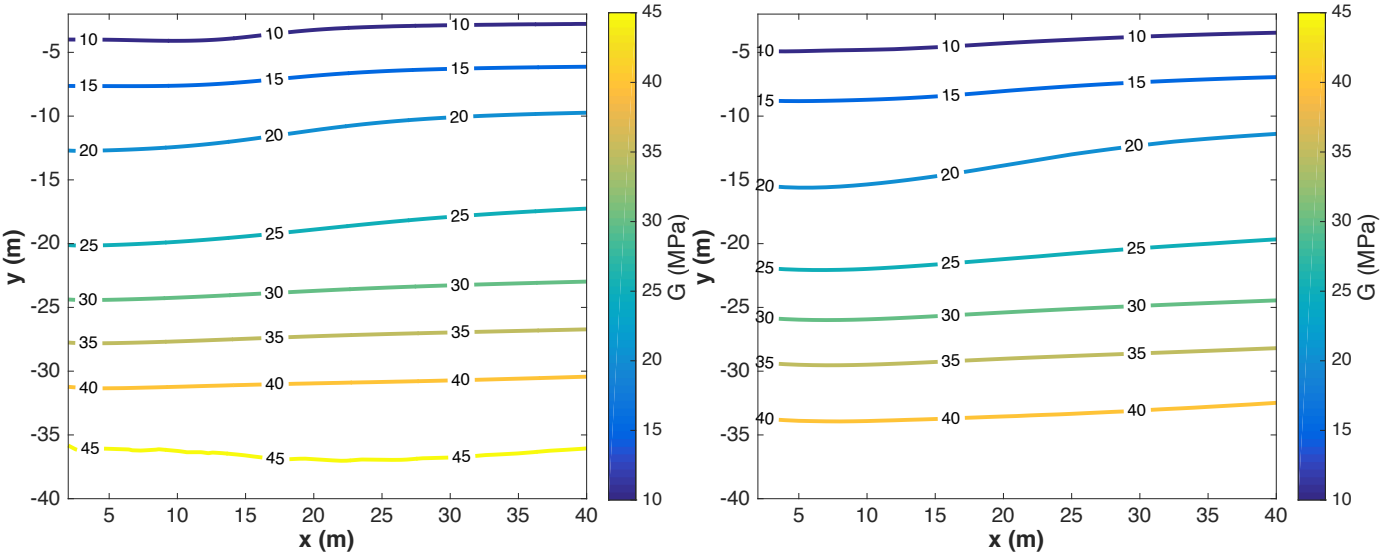

Figure C.1: G distribution for after 150 days (left) and after 1 years (right)

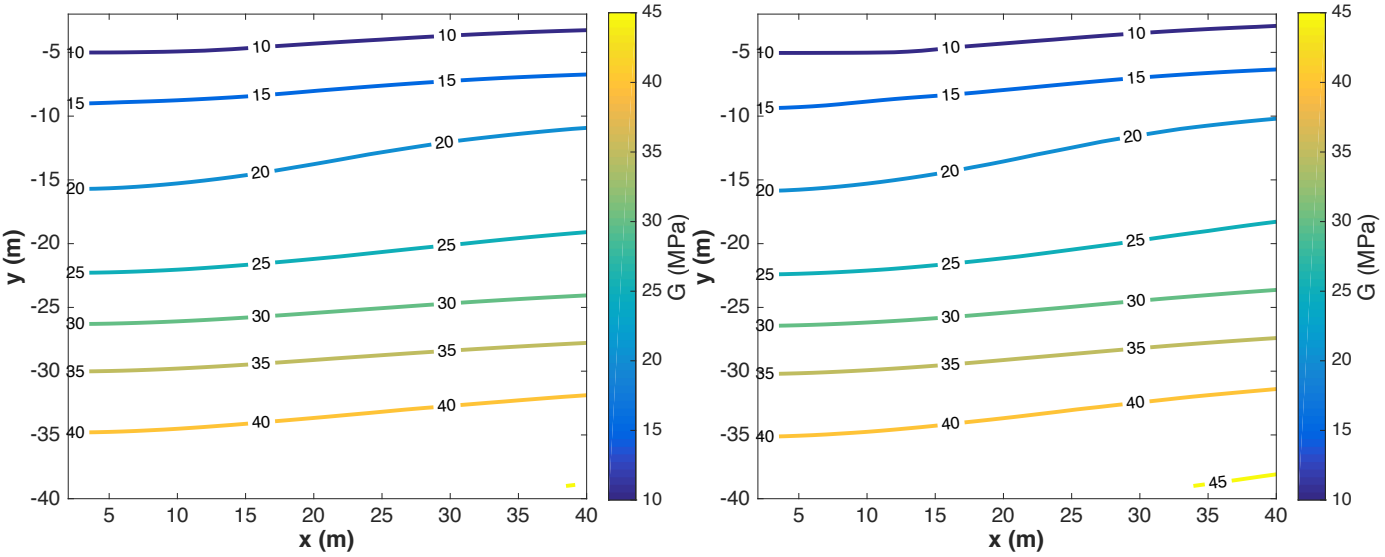

Figure C.2: G distribution for after 20 year (left) and after 120 years (right)

C.5 Loss factor distribution in the combined model

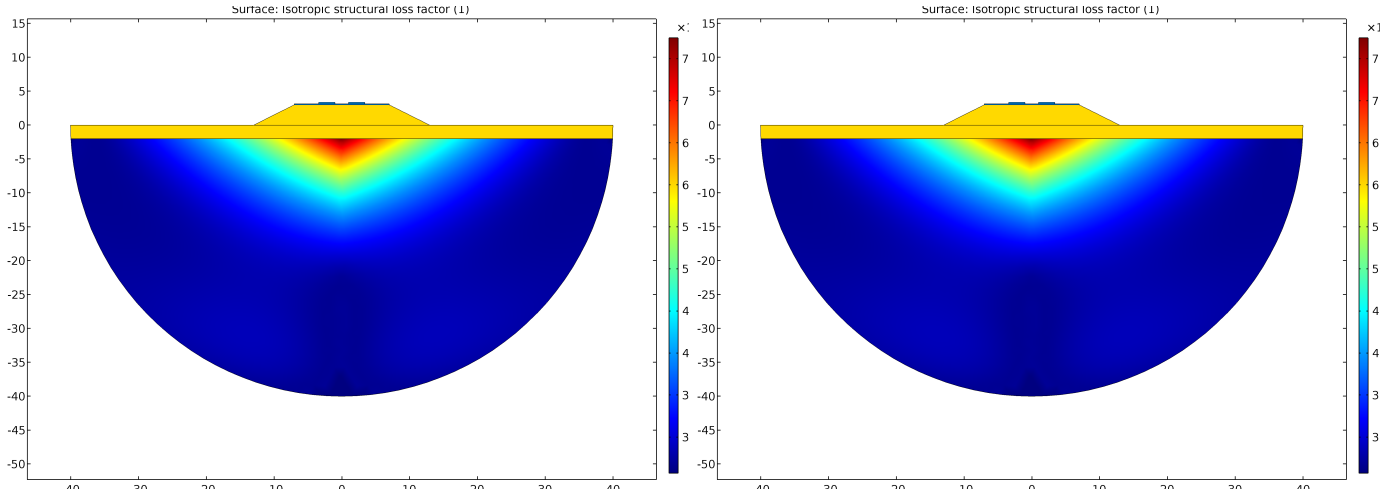

Figure C.3: Loss factor distribution for after 150 days (left) and after 1 years (right)

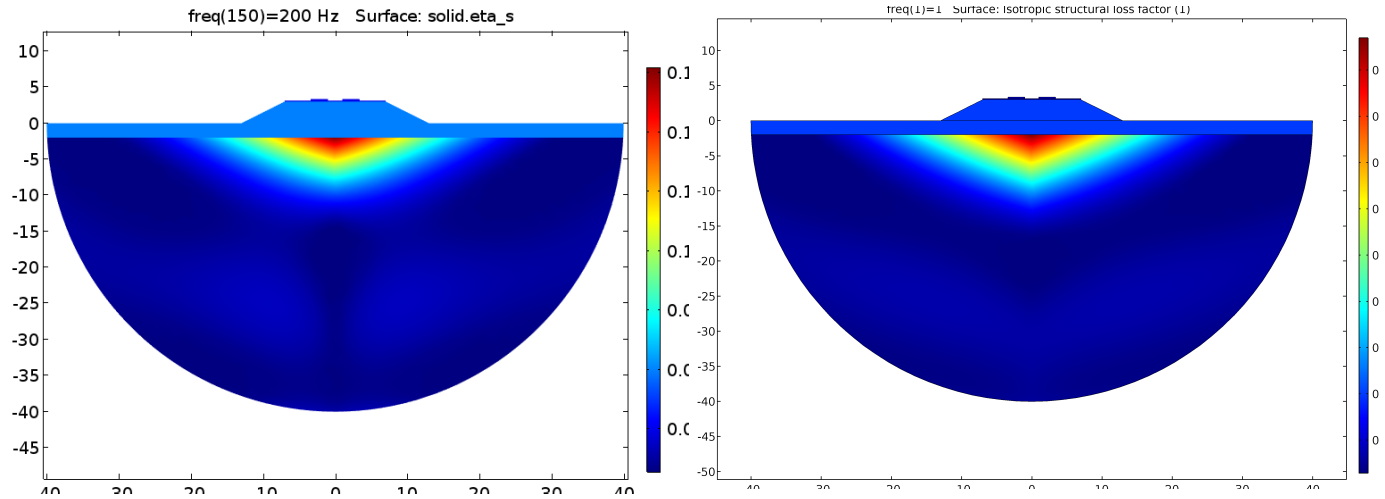

Figure C.4: Loss factor distribution for after 20 year (left) and after 120 years (right)